FINAL REPORT
(September 3, 1974 through October 23, 1975)

on

Cont act NAS8-31007
STUDY OF GROWTH OF SINGLE CRYSTAL RIBBON IN SPACE

to

NATIONAL AERONAUTICS AND SPACE ADMINISTRATION
MARSHALL SPACE FLIGHT CENTER

by

Van E. Wood and Alan J. Markworth

October 30, 1975

BATTELLE
Columbus Laboratories
505 King Avenue
Columbus, Ohio 43201

TABLE OF CONTENTS

LIST OF FIGURES

LIST OF FIGURES
(Cont.)

LIST OF TABLES

PREFACE

This report was prepared by Battelle-Columbus Laboratories under Contract NAS8-31007, "Study of Growth of Single-Crystal Ribbon in Space", for the George C. Marshall Space Flight Center of the National Aeronautics and Space Administration.

The report was written by Dr. Van E. Wood, Solid State and Optical Sciences Section, and Dr. Alan J. Markworth, Metal Science Section. Others contributing to the work were Dr. R. P. Kenan and Dr. A. E. Austin of Battelle-Columbus, and Dr. William Oldfield, consultant from Materials Research and Computer Simulation, Westerville, Ohio. The program's technical monitor (COR) at NASA-MSFC was Rudolph C. Ruff.

SUMMARY

A study is presented of the technical feasibility of growing single-crystal silicon ribbon in space environment. Electromagnetic shaping and other shaping processes are considered in separate tasks Procedures are described for calculating the electromagnetic fields produced in a silicon ribbon by an rf shaping coil. From a knowledge of these fields, the forces on the ribbon and the degree of shaping to be expected are determined. The expected steady-state temperature distribution in the ribbon is calculated in the one-dimensional approximation. It is indicated that shaping coil current required has in the past frequently been underestimated, currents in 100 A range being needed to produce ribbon of 0.4 mm thickness, even with very small shaping coils very close to the melt. The power requirements for shaping an isolated ribbon are rather large,by the standards of near-term space missions, but for shaping to 0.4 mm a ribbon being drawn from a free-floating spherical melt, the power required is in the range of a few kilowatts which does not seem excessive. Calculations on simplified models indicate, however, that lack of flatness of the shaped ribbon and excessive heating of the melt by the eddy currents induced by the shaping fields may pose problems An analysis of the relative effects of various kinds of forces other than electromagnetic showed that in the space environment capillarity forces would dominate, and that the shape of the melt is thus principally determined by the shape of any solids with which it comes in contact This suggests that ribbon may be produced simply by drawing between parallel wires A concept has been developed for a process of off-angle growth, in which the ribbon is pulled at an angle to the solidification front. If it could be implemented, such a process promises to offer increased growth rate, better homogeneity, and thinner ribbon. While we recommend that work on development of concepts for space processing of silicon ribbon be continued to the extent consistent with the overall goals of the space-processing program, we do not recommend further terrestrial experimental work because of the highly space-oriented nature of the most promising concepts.

FINAL REPORT

on

STUDY OF GROWTH OF SINGLE CRYSTAL RIBBON IN SPACE

to

NATIONAL AERONAUTICS AND SPACE ADMINISTRATION
MARSHALL SPACE FLIGHT CENTER

by

Van E. Wood and Alan J. Markworth

October 30, 1975

BATTELLE
Columbus Laboratories

1. INTRODUCTION

1.1 Background

From almost every aspect, the least satisfactory part of the process of manufacturing silicon single-crystal wafers, whether for integrated-circuit or solar-cell application, is the cutting and polishing of the wafers from the crystal boules. The process is expensive, requires skilled hand work, wastes at least half the crystal, and introduces strain and heavy-metal impurities into the finished wafers. Consequently, there has been considerable interest in developing methods of producing single-crystal ribbons or films directly. In this report, we describe investigations into some aspects of whether processing in a space environment might be a feasible and useful method of producing silicon single-crystal ribbon. A little interest also attaches to other semiconductors, but inasmuch as silicon is by far the most widely used material for integrated circuits and is the prime candidate for photovoltaic cells for large-scale power conversion, it will be the only material specifically discussed. Some other work has been done along these

lines. A program at Texas Instruments[1] looked into electromagnetic shaping of silicon ribbon; it involved some terrestrial experiments which were not too successful. A more recent program[2] at McDonnell-Douglas is devoted to a conceptual and economic study of an overall space processing system. In this proposed system, electromagnetic shaping is again used, but the ribbon is drawn from a continually repelenished levitated sphere. This concept is very nicely adapted to space processing. We shall describe aspects of these programs in some more detail later.

1.2 Organization of Program and of Report

This is the final report on a program involving three separate tasks, the first two of which were carried out separately. The first task was a study of electromagnetic shaping, including development of methods of calculation of the electromagnetic fields, forces, and power requirements, and thermal effects involved. This work is described in Section 2, where we show among other things that the current needed for electromagnetic shaping has generally been rather underestimated in previous work. In the second task, we examined other possible space-processing methods and isolated the principal factors involved in space growth of single-crystal ribbon. The results of this investigation and a suggested method for drawing ribbon in space are described in Section 3. The third task, discussed in Section 4, was an assessment of the overall technical prospects for space production of silicon ribbon and a recommendation of the directions future work might profitably take.

Several areas were specifically excluded from consideration because it was felt investigation of them would be premature:

1. mechanical stability against dynamic perturbations,
2. degree of crystallinity and perfection of ribbon produced (except for a few general comments),
3. economic feasibility of any process.

In this report, equations and figures are numbered separately for each section, using a multiple decimal system, in order to avoid excessive renumbering. Thus, Eq. (2.3.1) refers to the first equation of section 2.3. The references, on the other hand, are numbered consecutively for the whole report to avoid excessive repetition. Since there are only a few tables, they too are numbered consecutively through the whole report.

1.3 Physical Properties of Silicon

In Table I we have collected, for convenience, representative data on the physical properties of silicon which are potentially useful in the study of crystallization and electromagnetic shaping in this material. Not all the data in Table 1 are essential to the calculations presented in this report, though. We have not attempted to make a complete literature survey or to determine a "best" value for the parameters, but we have insofar as possible selected experimental results determined near the melting temperature in both the solid and liquid phases. These data will be entirely accurate enough for the present studies. Here,and throughout the report, SI units will be used.

We shall adopt the following convention for the symbols referring to these data: symbols without a subscript will refer to the liquid phase; symbols referring to the solid phase will have a subscript "s".

The thermal diffusivities, $\kappa = K/C\Delta$, calculated from the Table I data are $\kappa = 3.0 \times 10^{-5}$ m^2/sec in the liquid state and $\kappa_s = 9.9 \times 10^{-6}$ m^2/sec for the solid. The latter value can be compared with an extrapolated estimate of 9.4×10^{-6} m^2/sec given by Touloukian et al[13]. These diffusivities are large, considering the small dimensions over which shaping of a ribbon is liable to take place; so in investigating thermal properties, it will not be necessary to consider other than steady-state conditions.

The surface tension, and consequently power required for shaping, might be reduced by heating the melt above the melting temperature, particularly at reduced pressure[2]. We will not consider this possibility in our numerical calculations, though.

TABLE I. TYPICAL VALUES OF PHYSICAL PROPERTIES OF SOLID AND LIQUID SILICON NEAR THE MELTING TEMPERATURE

Property and Symbol	Value		Refs.
	Liquid	Solid	
Melting temperature, T_m	1685 K		3
Latent heat of fusion, L	$1.80\ MJ\ kg^{-1}$		3
Density, Δ	$2.49 \times 10^3\ kg\ m^{-3}$	$2.29 \times 10^3\ kg\ m^{-3}$	4
Thermal conductivity, K	$67.\ W\ m^{-1}\ K^{-1}$	$22.0\ W\ m^{-1}\ K^{-1}$	5,6
Specific heat, C	$9.12 \times 10^2 J\ kg^{-1}K^{-1}$	$9.73 \times 10^2\ J\ kg^{-1}K^{-1}$	3
Resistivity, ρ	8.3×10^{-7} ohm m	1.7×10^{-5} ohm m	7
Surface tension, γ (or surface free energy)	$0.72\ N\ m^{-1}$	$1.23\ N\ m^{-1}$ ({111}plane)	8,9
Viscosity, μ	$2.0 \times 10^{-3}\ N\ sec\ m^{-2}$		10
Emissivity, ε	0.5 (rough estimate)	0.6 (extrapolation)	11,12

2. ELECTROMAGNETIC SHAPING

2.1 Statement of Problem

The objectives of this portion of the program are the development of analytical techniques and calculational procedures, including computer programs, for determining electromagnetic fields and forces and temperature changes within a column of molten silicon being shaped into a thin ribbon by eddy-current forces induced in the silicon by an external shaping coil; determining the power requirements and degree of shaping that may be obtained for given configurations and dimensions of the shaping coil; and assessing effects of the freezing of the shaped ribbon near the shaping position. Electromagnetic shaping is obviously attractive as a potentially contamination-free shaping method, and appears particularly attractive for use in space, where there will be no difficulties with convection in the melt. Moreover, it has generally been considered, apparently on the basis of the early estimates of Gaule' and Pastore[14], that the power requirements for electromagnetic shaping to submillimeter thickness were quite moderate. If the ribbon were drawn in space from a large levitated sphere, as in the McDonnell-Douglas concept[2], further savings in required power might be anticipated because of the removal of the constraint of constant cross-sectional area of the molten zone which the gravitational field effectively imposes on earth.

One might in principle attempt to solve the electromagnetic problem in a completely general way for a given coil configuration by assuming some reasonable shape for the molten ribbon, calculating the eddy currents and force distribution for this shape, allowing the shape of the melt to be modified slightly in the direction indicated by the force distribution, recalculating the currents and forces, and so forth, until the increase in surface free energy of the melt on further shaping just balances the electromagnetic work necessary to achieve that shaping. Actually we shall follow a program rather like this, but to avoid having to solve an extremely complicated three-dimensional eddy-current problem, in conjunction with a free variational problem to determine the shape of the melt, we will make what we believe are

reasonable assumptions about the geometry of both the shaper and the ribbon. This will also enable us to identify more readily the factors of primary importance in determining the effectiveness of the shaping process. In return, we give up in principle, though not in practice, since the exact problem would surely prove wholly intractable, some knowledge about the exact shape of the frozen ribbon.

As far as the shaping coil goes, it is clear that it is sufficient to consider it as made up of pairs of straight wires running parallel to the flattened surfaces of the ribbon and perpendicular to the pulling direction, and symmetrically disposed across the melt, since wires running in any other directions will not be effective in producing ribbon of the desired shape. Moreover, it will be adequate to consider one pair of such wires, since the field distribution from a group of shaping wires can be obtained by adding vectorially the fields from each constituent. Thus we shall largely concentrate our attention on a single hairpin-shaped coil, with the bend sufficiently remote from the ribbon to have negligible influence, disposed as described above (and illustrated in Figs. 2.3.1, 2.3.2, and 2.4.1). We will neglect any effects of the induced fields back on the shaper, which after all carries a very high current. The single hairpin shaping coil is also very important as a limiting case; for a given total input current and a given distance b of closest approach of coil to melt, it is easy to see that no greater degree of shaping can be obtained than can be gotten by putting all the current into a single coil at the distance b. Some more complex configuration may have some other desirable feature, such as shaping effectively over a greater ribbon length, but for a given ribbon thickness, it will take more current.

As for the ribbon, we shall assume that it is drawn in such a way that in the critical shaping region its broad sides are reasonably flat and "vertical"--that is, perpendicular to the plane of the shaping coil. Calculations on surface energy of melt-ribbon configurations[11,14] seem to indicate that such a configuration can be obtained with a shaping coil similar

to that described above. Of course the coil must then be interacting significantly with the non-"vertical" portion of the liquid, but we must ignore this in the interests of simplicity. It does seem[11] that there are circumstances where this is not at all a bad approximation. Another approximation is that any possible change of ribbon shape between the plane of the shaper, where the electromagnetic force is greatest, and the freezing plane is ignored. It might be possible under some circumstances to arrange the pull rate so that the flat ribbon shape was maintained, but one would not wish to rely on this. Finally, we assume the ribbon is very broad in comparison to its thickness, as it appears it will have to be[2] for satisfactory productivity; so it will be a good approximation to assume that the fields, forces, etc., do not vary along the broad dimension of the ribbon. This is a tremendous simplification, since it reduces a fully three-dimensional problem to a two-dimensional one. (There may still be field components in all directions, but they do not vary along one). To our knowledge, no three-dimensional eddy current problem of comparable complexity has ever been solved, numerically or otherwise. The flat ribbon would presumably be terminated by little caps of semicircular cross-section (Fig. 2.4.1); although these may be important in determining the surface energy, the shaping field effects on them can be neglected. Originally we attempted to avoid the flat ribbon assumption by assuming the ribbon cross section was that of an elongated ellipse. Eventually, however, we realized that this only complicated the problem without giving much in return; in particular, it is much harder to consider the effects of the freezing interface if the ribbon is not flat. The effects of the various approximations are discussed qualitatively, and to some extent quantitatively, elsewhere in the report.

When specific ribbon dimensions are needed for purposes of numerical calculation, we shall assume a ribbon width of 6 cm and thickness 400 μm. The same values are generally used for illustration in the McDonnell-Douglas report[2]. For solar cell applications, somewhat thinner ribbon-say 250 μm--would be desirable; in the ribbon-from-levitated-sphere setup, though, the amount of extra power required to achieve the lesser thickness does not ordinarily appear to be very great.

2.2 Basic Electromagnetic Equations

In this section we give, without derivations, the basic equations for determining the eddy current density in and induced force distribution on a metallic melt in the field of external shaping coils. SI (mksA) units are used. A single exciting frequency will be assumed; generalization is straightforward. A superscript 0 will be used to indicate values of various quantitities in the "vacuum" region outside the molten zone; no superscript will indicate values inside the melt. We discuss first the molten ribbon and the space around it. When we come to discuss the solidified ribbon and the solid-liquid interface, we will use a superscript "s" for fields and forces within the solid region. A tilde (~) underneath a letter will be used to designate a vector quantity.

For a single driving frequency $f = \omega/2\pi$, and neglecting, as usual in eddy-current problems, small displacement current terms, the independent Maxwell equations to be solved are:

Inside	Outside	
$\nabla \times \underset{\sim}{E} = -i\mu_0 \omega \underset{\sim}{H}$	$\nabla \times \underset{\sim}{E}^0 = -i\mu_0 \omega \underset{\sim}{H}^0$	(2.2.1a,b)
$\nabla \times \underset{\sim}{H} = \sigma \underset{\sim}{E}$	$\nabla \times \underset{\sim}{H}^0 = 0$	(2.2.2a,b)
	$\nabla \cdot \underset{\sim}{E}^0 = 0$	(2.2.3)

where σ is the conductivity of the molten material, and $\underset{\sim}{E}$ and $\underset{\sim}{H}$ denote the steady parts of the electric and magnetic fields; that is, $\underset{\sim}{E}(t) = \underset{\sim}{E} e^{i\omega t}$, for example. The usual procedure of taking the curl of the curl equations leads to the vector Helmholtz equations (inside) and vector Laplace equations (outside)

$\nabla^2 \underset{\sim}{E} = (2i/\delta^2)\underset{\sim}{E}$	$\nabla^2 \underset{\sim}{E}^0 = 0$	(2.2.4a,b)
$\nabla^2 \underset{\sim}{H} = (2i/\delta^2)\underset{\sim}{H}$	$\nabla^2 \underset{\sim}{H}^0 = 0$	(2.2.5a,b)

where the skin depth $\delta = (2/\mu_0 \omega \sigma)^{1/2}$.

In the solid, the corresponding Maxwell and Helmholtz equations will naturally be of the same form as (2.2.1a,2a,4a,5a), but with σ replaced by σ_s, the solid conductivity, and δ by δ_s, the skin depth in the solid.

The skin depths δ and δ_s are among the most important physical parameters of our problem (or of any eddy-current problem). To provide an idea of orders of magnitude, we note the numerical relationship

$$4.737f = 10^6 \delta^{-2} \quad , \tag{2.2.6}$$

where f is in MHz and δ in μm. Thus for example for an operating frequency of 21.1 MHz, the skin depth in the melt will be 100 μm. At the same frequency, the skin depth δ_s in the solid will be about 455 μm. The boundary conditions to be satisfied at the melt-vacuum interface are

For the electric field	For the magnetic field	
$\underset{\sim}{E}_t = \underset{\sim}{E}_t^0$	$\underset{\sim}{H}_t = \underset{\sim}{H}_t^0$	(2.2.7a,b)
$(\nabla \times \underset{\sim}{E})_t = (\nabla \times \underset{\sim}{E}^0)_t$	$(\nabla \times \underset{\sim}{H}^0)_t = 0$	(2.2.8a,b)
$\underset{\sim}{E}_n = \underset{\sim}{E}_n^0$	$\underset{\sim}{H}_n = \underset{\sim}{H}_n^0$	(2.2.9a,b)

where subscripts t and n denote as usual components tangential and normal to the surface, respectively. Not all these conditions are independent. At the solid-liquid boundary, the same equations hold if superscript "0" is replaced by "s". Additional boundary conditions, at large distances from the ribbon and at the ribbon's center, are discussed where they are specifically needed.

The eddy current density in the melt may be determined from Ohm's law

$$\underset{\sim}{j} = \sigma \underset{\sim}{E} \quad , \tag{2.2.10}$$

and the steady force density on the melt found from

$$\underset{\sim}{f} = \frac{\mu_0}{2} \operatorname{Re} (\underset{\sim}{j} \times \underset{\sim}{H}^*) \quad . \tag{2.2.11}$$

If we define a complex Poynting vector by

$$\underset{\sim}{S} = 1/2\ (\underset{\sim}{E} \times \underset{\sim}{H}^{*}) \quad , \tag{2.2.12}$$

and then define

$$\Pi = - \int \underset{\sim}{S} \cdot \hat{n}\, dA \quad , \tag{2.2.13}$$

where the integral is taken over the surface of the ribbon and $\hat{n}$ denotes an outward normal to that surface, then Re Π is the steady Ohmic power loss in the ribbon and Im Π is 2ω times the average magnetic energy stored in the ribbon[15]. At the input of the shaper coil, the effect of the eddy currents is thus to provide an additional impedance $Z_e = 2\Pi/I^2$, where I is the peak current in the coil.

2.3 Fields and Forces in Uniform Ribbon

In this section we investigate the forces exerted on a semi-infinite region of a uniform metallic material (such as liquid Si) by a single long straight wire carrying alternating current of peak value I. The wire is parallel to the surface of the metallic half-space, which we shall refer to as the melt, although a real molten metal would of course be deformed away from the wire. Thus, the principal assumption in addition to those made previously is that the liquid-solid interface is far enough away from the shaping region that it can be ignored. Techniques to avoid having to make this assumption are described in Section 2.6, and its region of validity is discussed in Section 2.7. Also, since we are really primarily interested in a thin ribbon rather than a semi-infinite region, the results of this section will only be strictly valid when the skin depth is small compared to the plate thickness t say $\delta < t/3$. This approximation will also be removed in Section 2.6. As we shall see, there may be conditions under which a relatively large skin depth may be desirable; but the results of this section will still be good first approximations at any reasonable operating frequencies.

Aspects of this problem have been studied before, particularly by Pritsky and Jerrard[16], and by Stoll[17]. The force distributions were not studied, though. Our simple method for obtaining the fields and forces at

the surface of the melt is also new. Furthermore, Stoll's account contains a good deal of incorrect mathematics. We have tried to clarify this part of the discussion. This relatively simple problem is very instructive in showing the general nature of the force distributions and the relevant combinations of parameters of interest.

The notation to be used is illustrated in Fig. 2.3.1. We call the wire-to-melt perpendicular distance b. The direction along which the melt is being drawn is x; this is made more apparent in Fig. 2.3.2, where the two-wire thin ribbon case is illustrated. By the assumed symmetry of the problem, no quantities can vary with z. The problem to be solved is therefore two-dimensional.

We also note that the magnetic field of the isolated straight wire has no component along the direction of current flow, (the z direction) and that the presence of the molten zone, with no variation along z either, cannot alter this. Thus our Maxwell equation $\nabla \times \vec{H} = \sigma \vec{E}$ inside the melt reduces to $\hat{k}[\partial H_y/\partial x - \partial H_x/\partial y] = \sigma \vec{E}$. So $\vec{E}$ inside the melt and, by continuity, outside has only a z-component. We can write the Maxwell equations in component form as

$$-i\mu_0 \omega H_x = \frac{\partial E_z}{\partial y} \tag{2.3.1a}$$

$$i\mu_0 \omega H_y = \frac{\partial E_z}{\partial x} \tag{2.3.1b}$$

$$\frac{\partial H_y}{\partial x} - \frac{\partial H_x}{\partial y} \begin{cases} = \sigma E_z \text{ inside} & (2.3.2a) \\ = 0 \text{ outside} & (2.3.2b) \end{cases}$$

Rather than using these equations and the associated boundary conditions directly, it will be convenient to follow Stoll and introduce the magnetic vector potential $\vec{A}$, defined by $\vec{B} = \mu_0 \vec{H} = \nabla \times \vec{A}$. For $\vec{H}$ not to vary in the z direction, the x- and y- components of $\vec{A}$ must be constants, which can be taken without loss of generality to be zero. Thus, we are left with

$$H_x = \frac{1}{\mu_0} \frac{\partial A_z}{\partial y} , \tag{2.3.3a}$$

$$H_y = -\frac{1}{\mu_0} \frac{\partial A_z}{\partial x} , \quad \text{and from (2.3.1a)} \tag{2.3.3b}$$

$$E_z = -i\omega A_z , \tag{2.3.3c}$$

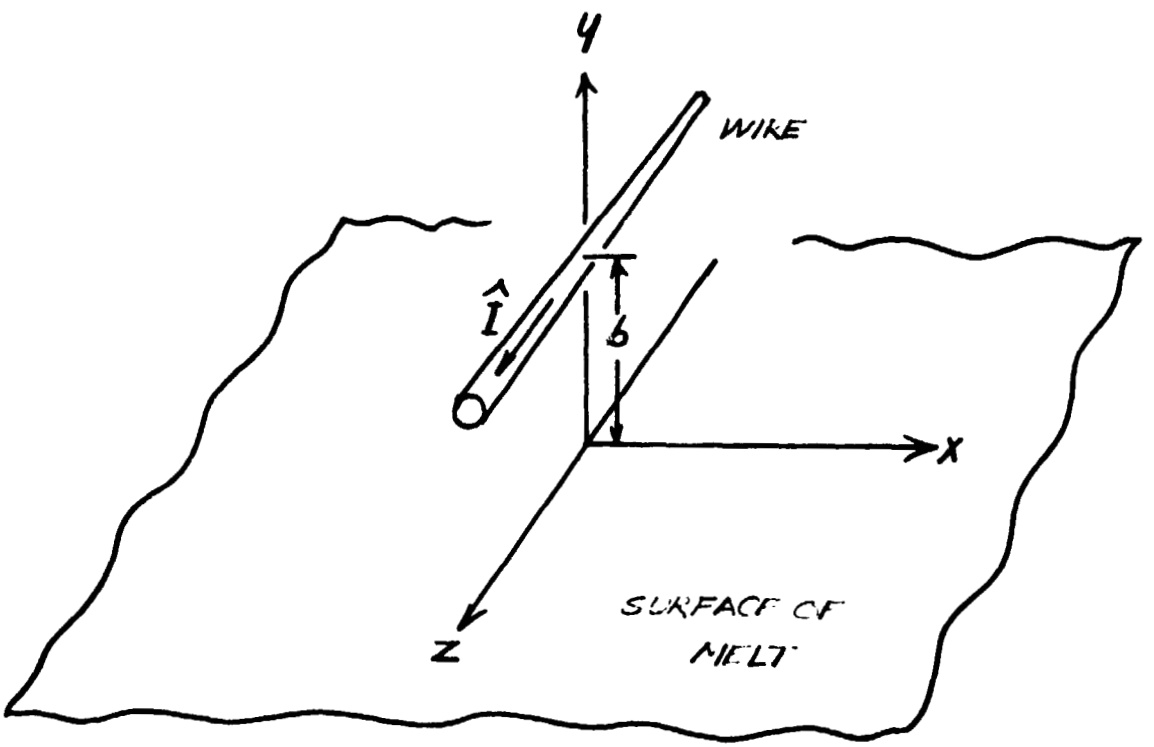

FIG. 2.3.1. PERSPECTIVE OF LONG STRAIGHT WIRE ABOVE SEMI-INFINITE MELT, SHOWING COORDINATE SYSTEM USED.

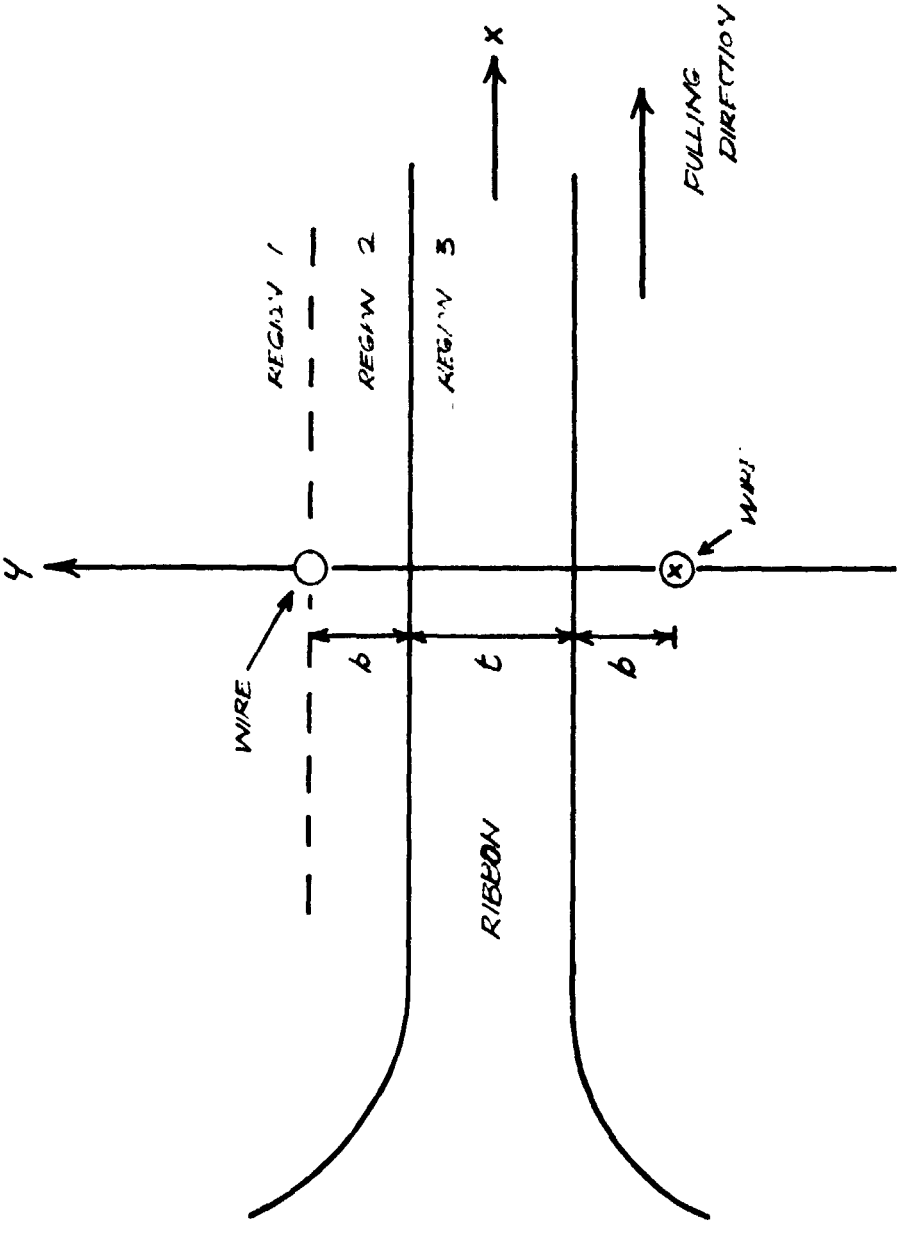

FIG. 2.3.2. SIDE VIEW OF FLAT RIBBON BEING SHAPED BY FORCES DUE TO TWO LONG STRAIGHT WIRES

where again an unimportant constant term has been dropped. Differentiating (3a) with respect to y, (3b) with respect to x, and using (2) and (3c) we get the Helmholtz equations for A_z,

$$\frac{\partial^2 A_3}{\partial x^2} + \frac{\partial^2 A_3}{\partial y^2} = \alpha^2 A_3 \text{ inside the melt,} \qquad (2.3.4a)$$

$$\frac{\partial^2 A_2}{\partial x^2} + \frac{\partial^2 A_2}{\partial y^2} = 0 \quad \text{outside,} \qquad (2.3.4b)$$

where we have indicated by A_3 the value of A_z inside the melt (region (3) in Fig. 2.3.2) and by A_2 the corresponding value just outside. In (2.3.4a), $\alpha^2 = 2i/\delta^2$. The boundary conditions at the surface of the melt (y = 0) can readily be obtained from those for $\vec{E}$ and $\vec{H}$. Continuity of E_z yields

$$A_2 = A_3, \; y = 0 \qquad (2.3.5a)$$

Continuity of H_x gives

$$\frac{\partial A_2}{\partial y} = \frac{\partial A_3}{\partial y}, \; y = 0 \qquad (2.3.5b)$$

Continuity of H_y provides no additional information. $A_z(x,y)$ must equal $A_z(-x,y)$ in order that $H_x(x,y) = H_x(-x,y)$ and $H_y(x,y) = -H_y(-x,y)$, as in the case of the isolated wire. Thus also $\partial A_z/\partial x = 0$ at $x = 0$.

We will solve Eqs. (2.3.4), together with boundary conditions (2.3.5) and appropriate conditions at infinity, by the Fourier transform method. Before doing this, however, it will be helpful to discuss the vector potential of the isolated current-carrying straight wire.

The vector potential $\vec{A}^{(is)}$ at (x,y) due to an isolated wire at (0,b) is given by

$$\vec{A}^{(is)}(x,y) = \frac{-\mu_o I \hat{k}}{4\pi} \ln (x^2 + (y-b)^2) + \vec{K},$$

where $\vec{K}$ is an arbitrary constant vector, independent of x and y. It is easily shown that this yields the usual formulas for the components of the

magnetic field of the isolated wire. As with the electrostatic potential, a constant term may be added since only differences in potential have physical significance. The difference in vector potential between two points of different y but the same x is clearly

$$\vec{A}^{(is)}(x,y_1) - \vec{A}^{(is)}(x,y_2) = \frac{-\mu_o I\hat{k}}{4\pi} \ln \frac{x^2+(y_1-b)^2}{x^2+(y_2-b)^2} \tag{2.3.6}$$

Consultation of a table of integrals (for instance, Eq. 1.4(2) of Erdelyi[18]) shows that (2.3.6) can also be written in the form

$$\vec{A}^{(is)}(x,y_1) - \vec{A}^{(is)}(x,y_2) = \frac{\mu_o I\hat{k}}{2\pi} \int_0^\infty \frac{dk}{k} \cos kx (e^{k(y_1-b)} - e^{k(y_2-b)})$$

for y_1 and $y_2 < b$. This integral is perfectly well behaved, but the separate exponential terms both diverge at the lower limit. However, we will not get into difficulty using such integrals to represent the vector potential of the isolated wire at a given point--that is,

$$\vec{A}^{is}(x,y) = \frac{\mu_o I\hat{k}}{2\pi} \int_0^\infty \frac{dk}{k} \cos kx\, e^{k(y-b)} ,$$

so long as we remember that only potential differences are physically significant.

Since $\vec{A}$ is an even function of x, a cosine transform on this variable is appropriate. We define

$$\bar{A}_i(k,y) = \int_0^\infty A_i(x,y) \cos kx\, dx, \quad i = 2,3 .$$

Multiplying Eq. (2.3.4) by cos kx and integrating on x, we find

$$\frac{\partial^2 \bar{A}_2}{\partial y^2} = k^2 \bar{A}_2 , \tag{2.3.7a}$$

$$\frac{\partial^2 \bar{A}_3}{\partial y^2} = (k^2 + \alpha^2)\bar{A}_3 \tag{2.3.7b}$$

Thus in general,

$$\bar{A}_2 = C_2 e^{ky} + D_2 e^{-ky} \tag{2.3.8a}$$

and

$$\bar{A}_3 = C_3 e^{\sqrt{k^2 + \quad}^2 y} + D_3 e^{-\sqrt{k^2 + \alpha^2} y} \quad , \tag{2.3.8b}$$

where it must be borne in mind that the coefficients C_2, C_3, D_2, D_3 can depend on k. In order that the solution be finite as $y \to -\infty$, we must have $D_3 = 0$. The Fourier Inversion Theorem thus gives

$$A_2(x,y) = \frac{2}{\pi} \int_0^\infty [C_2(k) e^{ky} + D_2(k) e^{-ky}] \cos kx \, dk \quad , \tag{2.3.9a}$$

$$A_3(x,y) = \frac{2}{\pi} \int_0^\infty C_3(k) e^{\sqrt{k^2 + \alpha^2} y} \cos kx \, dk \quad . \tag{2.3.9b}$$

When $\alpha \to 0$—that is, when the skin depth δ becomes infinite—these results must go over to those for the isolated wire; that is

$$A_i \to \frac{\mu_0 I}{2\pi} \int_0^\infty \frac{e^{-kb}}{k} e^{ky} \cos kx \, dk, \quad \alpha \to 0, \quad i = 2,3.$$

This can be achieved if

$$D_2 \to 0, \quad \alpha \to 0 \quad ;$$

$$C_3 \to C_2, \quad \alpha \to 0; \text{ and}$$

$$C_2(k) = \frac{\mu_0 I}{4} \frac{e^{-kb}}{k} \quad .$$

$C_2(k)$ must be independent of α for the vector potential to approach that for the isolated wire at large b. Inserting (2.3.9) into (2.3.5), we see

$$C_2 + D_2 = C_3 \quad .$$

$$k(C_2 - D_2) = \sqrt{k^2 + \alpha^2}\, C_3 \quad .$$

Thus, we finally obtain

$$A_2(x,y) = \frac{\mu_o I}{2\pi}\int_0^\infty \left[\frac{e^{k(y-b)}}{k} + e^{\frac{-k(y+b)}{k}}\,\frac{k-\sqrt{k^2+\alpha^2}}{k+\sqrt{k^2+\alpha^2}}\right]\cos kx\,dk, \qquad (2.3.10a)$$

$$A_3(x,y) = \frac{\mu_o I}{\pi}\int_0^\infty \frac{e^{\sqrt{k^2+\alpha^2}\,y-kb}}{k+\sqrt{k^2+\alpha^2}}\,dk. \qquad (2.3.10b)$$

From Eqs. (2.3.10), all the fields forces, etc., of interest can be calculated if the integrals can be evaluated. The integrands of A_2 and A_3 are finite and integrable everywhere in the range of integration.

From (2.3.3) and (2.3.10b) we can find the field components inside the metallic region

$$E_z = \frac{-i\mu_o\omega I}{\pi}\int_0^\infty \frac{e^{\sqrt{k^2+\alpha^2}\,y-kb}}{\sqrt{k^2+\alpha^2}+k}\cos kx\,dk \quad ; \qquad (2.3.11)$$

$$H_x = \frac{I}{\pi}\int_0^\infty \frac{\sqrt{k^2+\alpha^2}\,e^{\sqrt{k^2+\alpha^2}\,y-kb}}{\sqrt{k^2+\alpha^2}+k}\cos kx\,dk \quad ; \qquad (2.3.12)$$

$$H_y = \frac{I}{\pi}\int_0^\infty \frac{e^{\sqrt{k^2+\alpha^2}\,y-kb}}{\sqrt{k^2+\alpha^2}+k}\,k\sin kx\,dk \quad . \qquad (2.3.13)$$

By multiplying the integrand by $\frac{\sqrt{k^2+\alpha^2}-k}{\sqrt{k^2+\alpha^2}-k}$, the alternative forms

$$E_z = \frac{I}{\pi\sigma}\int_0^\infty e^{\sqrt{k^2+\alpha^2}\,y-kb}\cos kx\,(k-\sqrt{k^2+\alpha^2})\,dk \quad ; \qquad (2.3.11')$$

$$H_x = \frac{I\delta^2}{2\pi i}\int_0^\infty e^{\sqrt{k^2+\alpha^2}\,y-kb}\cos kx\,(k^2+\alpha^2-k\sqrt{k^2+\alpha^2})\,dk; \qquad (2.3.12')$$

$$H_y = \frac{-I\delta^2}{2\pi i}\int_0^\infty e^{\sqrt{k^2+\alpha^2}\,y-kb}\sin kx\,(k^2-k\sqrt{k^2+\alpha^2})\,dk \qquad (2.3.13')$$

can be obtained.

These forms are useful when b/δ is large. Numerical calculations[16,17] show that the fields fall off very rapidly (faster than $\exp(-|y|/\delta)$) inside the melt. The force distribution, depending on a product of electric and magnetic fields, falls off more rapidly still. Thus it seems appropriate to concentrate our attention on the fields and forces at the surface of the melt, where they are largest; however, by (2.2.13), these fields are all that are needed to calculate the power requirements.

At the surface, we have

$$E_z(0) = \frac{-i\mu_0\omega I}{\pi}\int_0^\infty \frac{e^{-kb}}{\sqrt{k^2+\alpha^2}+k}\cos kx\, dk \quad ; \tag{2.3.14}$$

$$H_x(0) = \frac{I}{\pi}\int_0^\infty \frac{e^{-kb}\cos kx\sqrt{k^2+\alpha^2}}{\sqrt{k^2+\alpha^2}+k}\,dk$$

$$= \frac{I}{\pi}\left[\int_0^\infty e^{-kb}\cos kx\, dk - \int_0^\infty \frac{e^{-kb}\cos kx\, k\, dk}{\sqrt{k^2+\alpha^2}+k}\right] \quad ; \tag{2.3.15}$$

$$H_y(0) = \frac{I}{\pi}\int_0^\infty \frac{e^{-kb}\,k\sin kx\, dk}{\sqrt{k^2+\alpha^2}+k} \quad ; \tag{2.3.16}$$

where $E_z(0)$ is short for $E_z(x,y=0)$, etc. These integrals can be evaluated in terms of certain generalizations of Bessel functions known as Struve functions[19], Bessel functions of the second kind, and elementary functions by writing the cos kx and sin kx terms in exponential form and using the known results[18]

$$\int_0^\infty \frac{dk\, e^{-pk}}{k+\sqrt{k^2+a^2}} = \frac{\pi}{2ap}\left(\underset{\sim}{H}_1(ap) - Y_1(ap)\right) - \frac{1}{a^2p^2} \quad , \tag{2.3.17}$$

and

$$\int_0^\infty e^{-bk}\cos kx\, dk = \frac{b}{b^2+x^2} \quad , \tag{2.3.18}$$

together with the result, obtained from (2.3.17) by differentiating with respect to the parameter p,

$$\int_0^\infty \frac{dk\, k\, e^{-pk}}{k+\sqrt{k^2+a^2}} = a\left\{\frac{\pi}{2ap}\,(H_2(ap) - Y_2(ap)) - \frac{1}{3} - \frac{2}{a^3p^3}\right\} \quad . \tag{2.3.19}$$

Eqs. (2.3.17) and (2.3.19) are valid for $\mathrm{Re}\ p > 0$, $|\arg a| < \pi/2$, conditions which are always fulfilled in the problem of interest here. In these equations, $\underset{\sim}{H}_1$ and $\underset{\sim}{H}_2$ are the Struve functions of the first and second orders. They should not be confused with Hankel functions which are also frequenty denoted by H's but without the tilde. (Also, although we used the tilde elsewhere to denote vectors, the Struve functions are of course not vectors).

We find that the fields at the surface can be expressed as

$$E_z(0) = \frac{\mu_0 \omega I}{2\pi}\left\{\frac{1}{\beta^2}\,\frac{1-\xi^2}{(1+\xi^2)^2} - \frac{\pi i}{2}\left[\frac{1}{\lambda_+}\,(\underset{\sim}{H}_1(\lambda_+) - Y_1(\lambda_+)) + \frac{1}{\lambda_-}(\underset{\sim}{H}_1(\lambda_-) - Y_1(\lambda_-))\right]\right\} \tag{2.3.20}$$

$$H_x(0) = \frac{I}{\pi b}\left[\frac{1}{1+\xi^2} - \frac{(1+i)\beta}{2}\left\{\frac{\pi}{2}\left[\frac{\underset{\sim}{H}_2(\lambda_+) - Y_2(\lambda_+)}{\lambda_+} + \frac{\underset{\sim}{H}_2(\lambda_-) - Y_2(\lambda_-)}{\lambda_-}\right] - \frac{2}{3} - \frac{1+i}{\beta^3}\,\frac{3\xi^2-1}{(1+\xi^2)^3}\right\}\right] \quad , \tag{2.3.21}$$

and

$$H_y(0) = \frac{I\delta}{\pi b^2}\left[\frac{i}{\beta}\,\frac{\xi(3-\xi^2)}{(1+\xi^2)^3} + \frac{(1-i)\pi\beta^2}{4}\left\{\frac{\underset{\sim}{H}_2(\lambda_-) - Y_2(\lambda_-)}{\lambda_-} - \frac{\underset{\sim}{H}_2(\lambda_+) - Y_2(\lambda_+)}{\lambda_+}\right\}\right] \quad , \tag{2.3.22}$$

where

$$\lambda_+ = \beta[(1-\xi) + i(1+\xi)] \quad , \tag{2.3.23a}$$

$$\lambda_- = \beta[(1+\xi) + i(1-\xi)] \quad , \tag{2.3.23b}$$

$$\beta = b/\delta \quad , \tag{2.3.23c}$$

and

$$\xi = x/b \quad . \tag{2.3.23d}$$

The variation in the complex variables $\lambda+$, $\lambda-$ as ξ increases from zero is sketched in Fig. 2.3.3. It should be noted that we have expressed each field in terms of the product of a coefficient which is similar to the field for the isolated wire and a function of the dimensionless variables β and ξ. Thus the most appropriate combinations of variables for studying the problem have been identified. Also, we may make use of the known properties of the Struve and Bessel functions to obtain in a straightforward way useful numerical results.

We could now write down general expressions for the force distribution at the surface, but we find it more convenient to consider first the fields in the large and small β regions.

For large β ($\beta \gg 1$), $\lambda+$ and $\lambda-$ will always be large in magnitude, and we may use the asymptotic expressions[19]

$$\underset{\sim}{H}_n(z) - Y_n(z) \approx \frac{1}{\pi} \sum_{m=0}^{\infty} \frac{\Gamma(m + 1/2)}{\Gamma(n-m + 1/2)(z/2)^{2m-n+1}} \quad .$$

These expansions are valid on the entire first sheet of the complex plane except for the negative real axis, which, as Fig. 2.3.3 shows, is never crossed. Alternatively, we can set $y = 0$ in Eqs. (2.3.11′-13′), and expand the remaining square roots. Either way, we obtain the asymptotic expansions

$$E_z(0) \sim \frac{-I}{\pi\sigma b\delta\,(1+\xi^2)}\left[1-\frac{1}{\beta}\,\frac{1-\xi^2}{1+\xi^2} + \frac{1}{2\beta^2}\,\frac{1-3\xi^2}{(1+\xi^2)^2} + i\left(1-\frac{1}{2\beta^2}\,\frac{1-3\xi^2}{(1+\xi^2)^2}\right)\right] , \quad (2.3.24)$$

$$H_x(0) \sim \frac{I}{\pi b}\,\frac{1}{1+\xi^2}\left[1 - \frac{1}{2\beta}\,\frac{1-\xi^2}{1+\xi^2} + i\left(\frac{1}{2\beta}\,\frac{1-\xi^2}{1+\xi^2} - \frac{1}{\beta^2}\,\frac{1-3\xi^2}{(1+\xi^2)^2}\right)\right] , \quad (2.3.25)$$

and

$$H_y(0) \sim \frac{I\delta}{\pi b^2}\,\frac{\xi}{(1+\xi^2)^2}\left[1-i\left(1-\frac{1}{\beta}\,\frac{3-\xi^2}{1+\xi^2}\right)\right] . \quad (2.3.26)$$

The next term in $H_y(0)$ is of order β^{-3}.

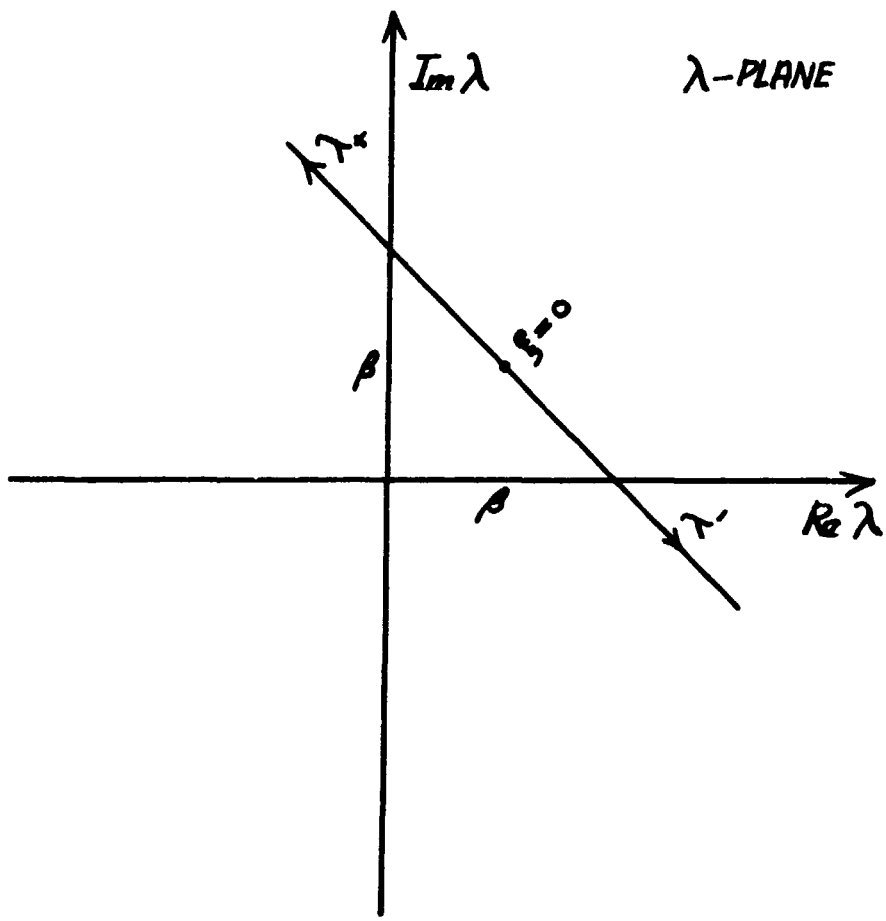

FIG. 2.3.3. THE COMPLEX λ-PLANE CUT ALONG THE NEGATIVE REAL AXIS, SHOWING THE VARIATION OF THE FUNCTIONS λ_+, λ_-, (EQS. 2.3.23a,b) WITH THE PARAMETER ξ. FOR ξ LESS THAN ZERO, λ_+ and λ_- ARE INTERCHANGED.

For small β—that is, for the wire very close to the melt—we can use expansions[19,20] of the $\underset{\sim}{H}$'s and $\underset{\sim}{Y}$'s valid for small values of the argument to obtain

$$E_z(0) = \frac{\mu_o \omega I}{2\pi}\left[-\frac{\pi}{4} + \frac{2}{3}\beta + i\left(\ln \beta\sqrt{\frac{1+\xi^2}{2}} + \left(\gamma - \frac{1}{2}\right)\right)\right] + \quad , \tag{2.3.27}$$

$$H_x(0) = \frac{I}{\pi b}\left[\frac{1}{2(1+\xi^2)} + \frac{\beta}{3} + i\left(\frac{\beta}{3}\right)\right] + \quad , \tag{2.3.28}$$

$$H_y(0) = \frac{I}{2\pi b}\frac{\xi}{1+\xi^2} + \quad . \tag{2.3.29}$$

In this case we have only displayed terms through β; the first neglected terms are proportional to β^2. Through terms in β, $H_y(0)$ is real.

Now by using the relation (Eq. (2.2.11))

$$\vec{f} = \frac{\mu_o}{2}\,\mathrm{Re}\,[\vec{j} \times \vec{H}^*] \quad ,$$

where

$$\vec{j} = \sigma \vec{E} \quad ,$$

we may find the force distribution at the surface in the two situations (large β and small β) for which we have given expressions for the field components. Since

$$\vec{E} = E_z \hat{k} \text{ and } \vec{H}^* = H_x^* \hat{i} + H_y^* \hat{j} \quad ,$$

the force distribution has in general two components, one normal to the surface

$$f_n = \frac{\mu_o \sigma}{2}\,\mathrm{Re}\,(E_z H_x^*) \quad , \tag{2.3.30}$$

and one tangential to the surface

$$f_t = \frac{\mu_o \sigma}{2}\,\mathrm{Re}\,(E_z H_y^*) \quad . \tag{2.3.31}$$

In the asymptotic ($\beta \gg 1$) regime, we find from Eqs. (2.3.24-26), (2.3.30) and (2.3.31), that

$$f_n(0) \sim \frac{-\mu_o I^2}{\pi^2 b^2 \delta} \frac{1}{(1+\xi^2)^2} \left[1 - \frac{1}{\beta} \left(\frac{1-\xi^2}{1+\xi^2} \right) + \frac{1}{2\beta^2} \frac{\xi^2}{1+\xi^2} \right] \quad , \tag{2.3.32}$$

$$f_t(0) \sim \frac{\mu_o I^2 \delta}{\pi^2 b^4} \frac{\xi}{(1+\xi^2)^4} \left[1 + \frac{1}{2\beta} \frac{1-3\xi^2}{1+\xi^2} \right] \quad . \tag{2.3.33}$$

There are several general observations that can be made about these force distributions:

1. f_n, as would be expected, is a force <u>on</u> the melt, tending to deform it away from the wire.
2. f_t is a stretching force, tending to pull the surface of the melt away from the line of closest approach.
3. Both force components fall off rapidly when $|\xi|$ becomes large.
4. The coefficients of β^{-1}, β^{-2}, etc., are bounded for large ξ; so it is clear the expansion is valid for large β for all values of ξ.
5. The maximum value of $|f_t|$ occurs approximately at $|\xi| = 1/\sqrt{7}$; the maximum of f_n is of course at $\xi = 0$.
6. For large β, the ratio of the tangential force to the normal force is very small. To be specific,

$$\frac{f_t(0)\ \max}{f_n(0)\ \max} \approx \frac{343\sqrt{7}}{4096} \frac{1}{\beta^2} \approx 0.2216 \frac{1}{\beta^2} \quad ;$$

so f_t max is less than 1 percent of f_n max for $\beta \geq 5$.

In Fig. (2.3.4), we have plotted $f_n(0)/(\mu_0 I^2/\pi b^2 \delta)$ as a function of the normalized distance along the pulling direction ξ for $\beta = 5$ and $\beta =$. It is obvious from the curves that this quantity depends only very weakly on β for $\beta \geq 5$, and tabulation or plotting for other β values in the asymptotic range is unnecessary. In Fig. (2.3.5), we plot $f_t(0)/(\mu_0 I^2/\pi^2 b^4)$

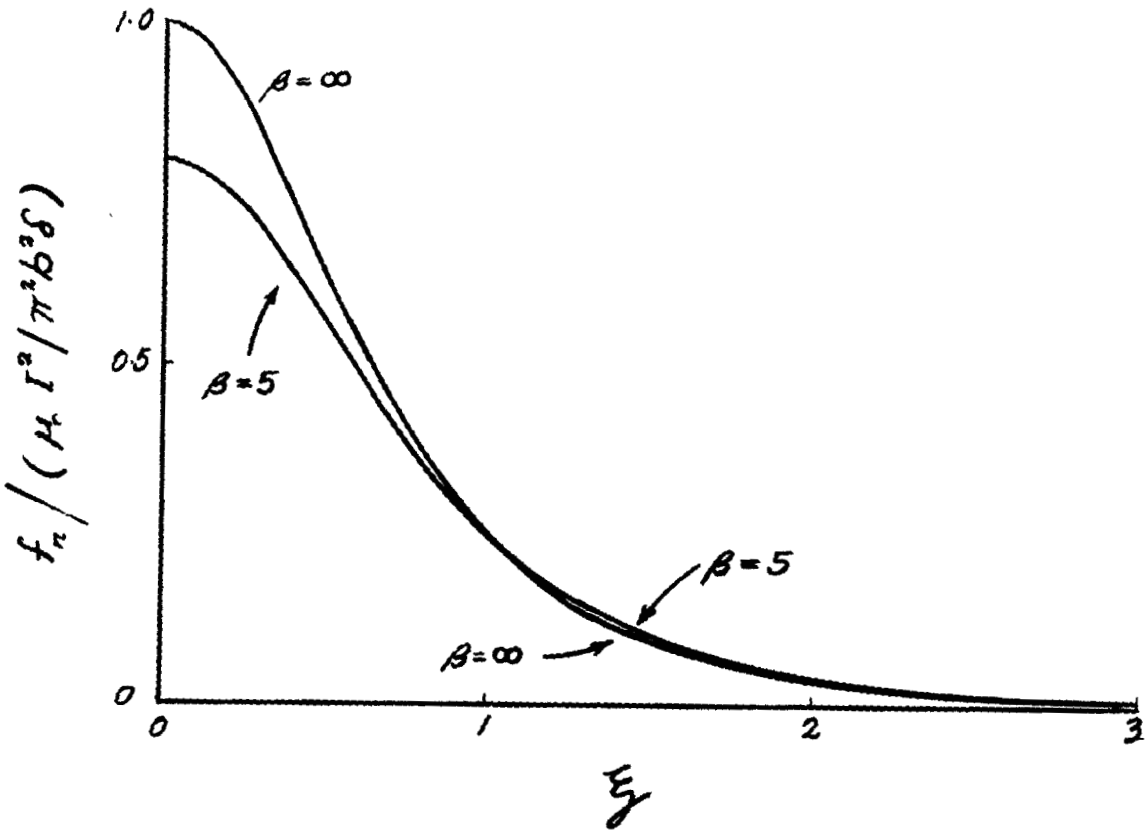

FIG. 2.3.4. NORMAL FORCE DENSITY AT MELT SURFACE, FOR TWO VALUES OF $\beta = b/\delta$, AS A FUNCTION OF $\xi = x/b$, THE NORMALIZED DISTANCE ALONG THE MELT AWAY FROM THE LINE OF CLOSEST APPROACH ($\xi = 0$) OF THE SHAPING WIRE. CURVES ARE SYMMETRICAL ABOUT $\xi = 0$.

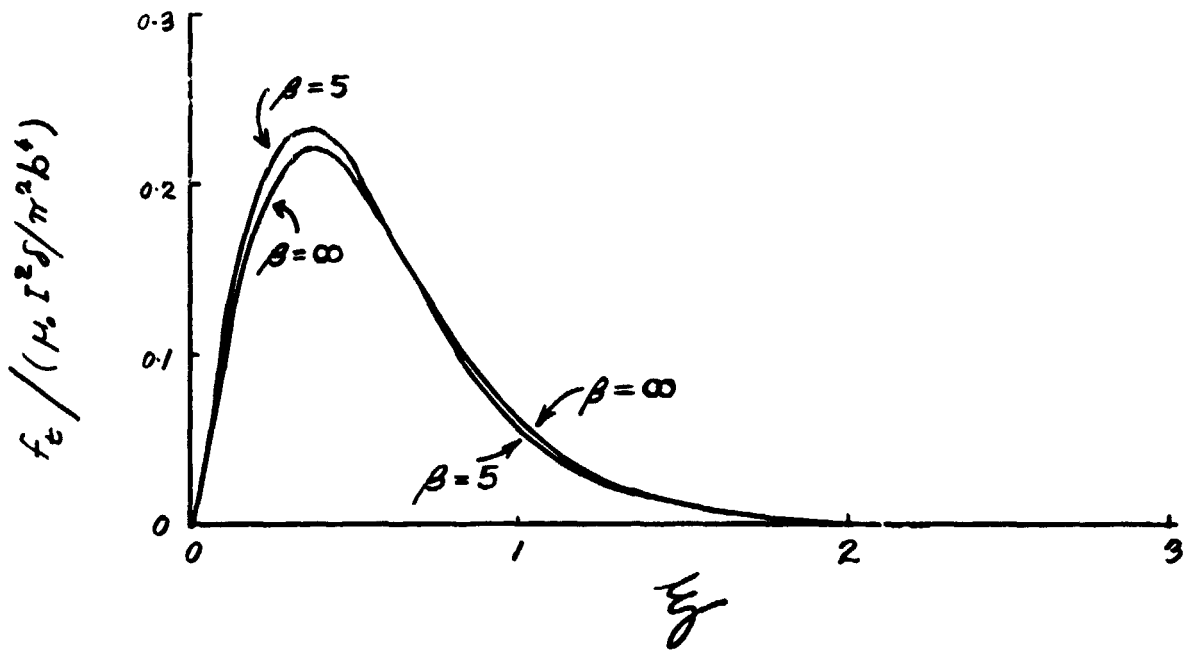

FIG. 2.3.5. TANGENTIAL FORCE DENSITY AT MELT SURFACE, FOR TWO VALUES OF $\beta = b/\delta$, AS A FUNCTION OF $\xi = x/b$, THE NORMALIZED DISTANCE ALONG THE MELT AWAY FROM THE LINE OF CLOSEST APPROACH ($\xi = 0$) OF THE SHAPING WIRE. CURVES ARE ANTI-SYMMETRICAL ABOUT $\xi = 0$.

vs. ξ, again for $\delta = 5$ and $\beta = \infty$. The same weak dependence on β is observed. While we have normalized the curves so as to plot quantities that are finite for large β, actually $f_n \to \infty$ and $f_t \to 0$ as $\beta \to \infty$ for fixed b. In Fig. (2.3.6), we plot on the same axes $f_n(0)/(\mu_0 I^2/\pi^2 b^3)$ and $f_t(0)/(\mu_0 I^2/\pi^2 b^3)$ vs. ξ for $\beta = 5$. In this graph, the forces are normalized to the magnitude of the total force exerted by the isolated wire on a test current at the corresponding point. The relative smallness of the tangential force is obvious.

In the small β ($\beta \ll 1$) regime, we find from Eqs. (2.3.27-31)

$$f_n(0) = \frac{-\mu_o I^2}{\pi b^3} \frac{\beta^2}{4} \left[\frac{1}{4(1+\xi^2)} + \left(\frac{1}{6} - \frac{2\gamma-1}{3\pi}\right)\beta - \frac{2\beta}{3\pi}\left(\frac{1}{1+\xi^2} + \ln\left(\frac{1+\xi^2}{2}\right)\right)\right], \tag{2.3.34}$$

$$f_t(0) = \frac{\mu_o I^2}{\pi b^3} \frac{\pi\beta^2}{16}\left(1 - \frac{8\beta}{3\pi}\right)\frac{\xi}{1+\xi^2}. \tag{2.3.35}$$

We notice the following features of these expressions:

1. The forces are in the same directions as they were for large β.
2. For given fixed values of b and ξ, the forces are much smaller for a given small value of β (say $\beta = 1/5$) than they were for a corresponding large value of β (say $\beta = 5$). This is simply because in the small-β case the force distributions extend into the melt.
3. The logarithmic term in f_n indicates that the expression (2.3.34) may not be valid for large ξ.
4. For moderately large ξ's, the tangential force may be relatively large, even larger than the normal force.
5. For fixed δ and very small b, the shaping force $f_{n\,max}$ only increases as $1/b$; while it increased as $1/b^2$ in the region where b was larger (Eq. (2.3.32)). Thus it seems probable that there is a point such that moving the wires in further to get a larger force will not be worthwhile, since the problems arising from any mechanical instabilities will be great, and the gain in shaping forces not so large. These remarks sufficiently describe the small-β situation so graphs of the force distributions will not be necessary, particularly since the regime where Eqs. (2.3.34-35) hold is not of great practical interest. Values of fields and forces for intermediate values of β could readily be obtained numerically if needed.

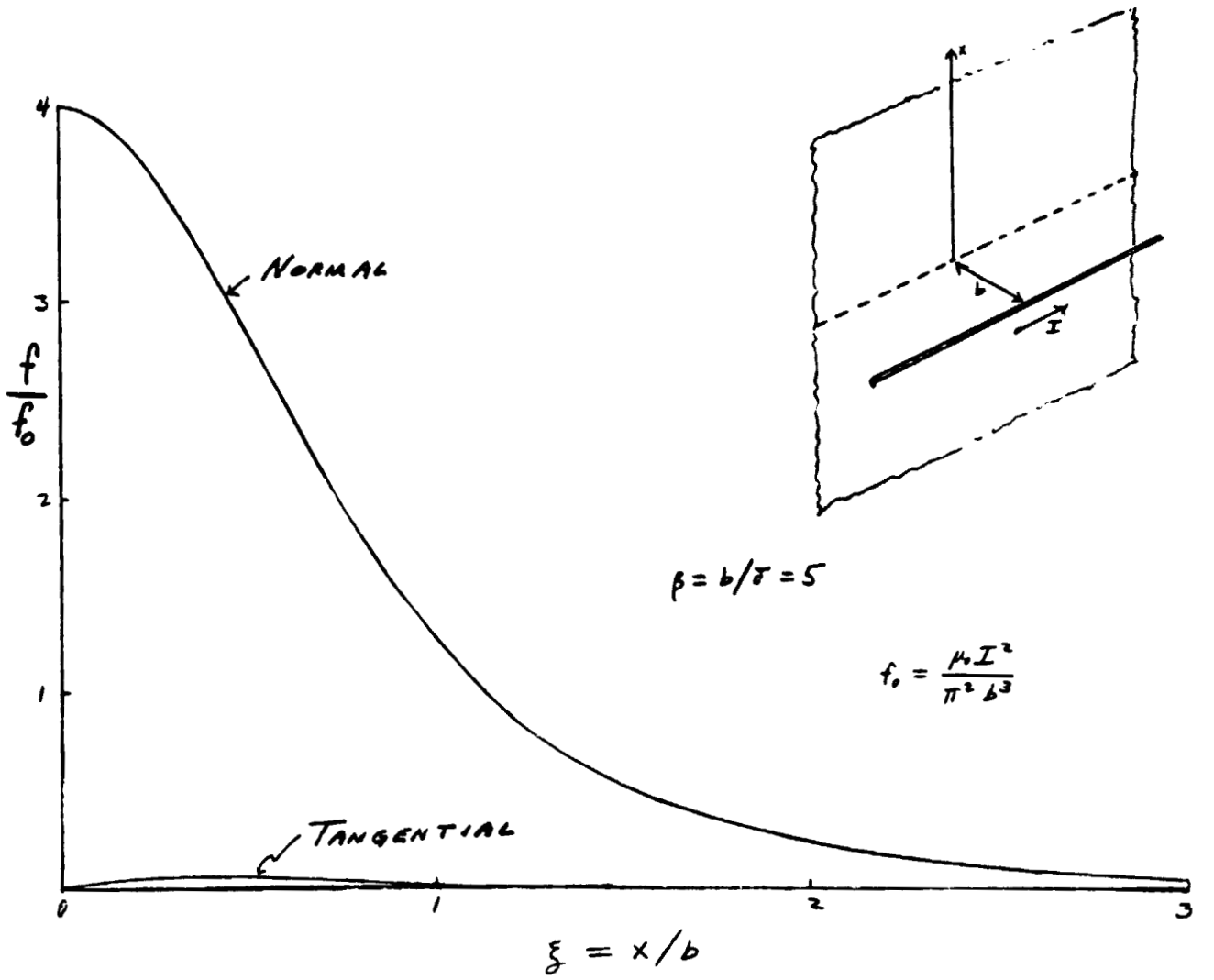

FIG. 2.3.6. NORMAL AND TANGENTIAL FORCE DENSITIES, NORMALIZED TO MAGNITUDE OF FORCE ON TEST CURRENT AT $\xi = 0$, FOR $\beta = 5$.

2.4 Determination of Degree of Shaping

2.4.1 Introduction

In this section, which for greater clarity will be divided into several subsections, we will develop expressions for the electromagnetic work done in changing the ribbon thickness, for the surface energy change with thickness, and for the shaper current required to shape the ribbon to a selected thickness. Power required for shaping is discussed in the following section. We shall consider first an isolated ribbon--a strip of liquid metal of fixed cross-sectional area extending a long way in both directions from the shaper--and then the McDonnell-Douglas RMGS setup[2], where the ribbon is pulled from a sphere of molten Si near the shaper. Aside from its analytical simplicity, the isolated ribbon case is important for several reasons:

1. The critical thickness-limiting factor for the isolated ribbon is the sharpening of the melt curvature at the ribbon edges. It has been necessary, owing to the complexity of the problem, to ignore this in the RMGS calculation[11]; so the isolated ribbon provides an opposite-limit approximation to the true intermediate situation.
2. In terrestrial experiments[1], gravity will tend to inhibit shape changes along the meniscus between the ribbon and the molten silicon supply. Thus, the cross-sectional area at the shaping level will be difficult to change and the shaping should be rather similar to that in the isolated ribbon.
3. Suggestions have been made for shaping thin ribbon by passing it through a series of progressively narrower coils, or by preliminarily shaping it by some other method and then finally thinning it electromagnetically. The isolated ribbon is clearly a good approximation to these situations.

The ultimate thickness of the ribbon is conveniently calculated by the energy balance method. As the ribbon becomes thinner, the change in surface free energy to shape it further increases--that is, it becomes more and more difficult to shape the thinner it gets. Meanwhile, the normal

electromagnetic force on the ribbon is less, the thinner it is, and there will be less and less electromagnetic energy available to do the work of further shaping. The thickness at which the free energy required for an infinitesimal further thinning is just equal to the electromagnetic work required to do this thinning will be the actual thickness of the ribbon in a given field. We first determine this ultimate thickness for a flat ribbon of finite width with circular-cylindrical terminations, such as discussed in previous work[1,14].

2.4.2 Surface Free Energy for Isolated Ribbon

We consider a ribbon of width W and thickness t, with curved ends of semicircular cross-section of radius t/2, as shown in Fig. 2.4.1. Most of the increase in surface energy on shaping comes from the end regions, which is why they must be included. If the central portion of the ribbon is indeed flat, this configuration with the semicircular ends will be that of lowest free energy. We will assume that the shaping takes place uniformly over a region of height H in the pulling direction; the shape of the normal force vs. distance curve along this direction (Fig. 2.3.4) ensures that this approximation(made implicitly by Gaule' and Pastore[14]) will be reasonably good. Then if we consider the ribbon being shaped from a width W_1 and thickness t_1 to a width W_2 and thickness t_2, the change in surface free energy is

$$\Delta E_s = \gamma H[(2W_2 + \pi t_2) - (2W_1 + \pi t_1)] \quad , \tag{2.4.1}$$

with the constraint

$$W_1 t_1 + \frac{\pi}{4} t_1^2 = W_2 t_2 + \frac{\pi}{4} t_2^2 \quad ,$$

where γ is the surface tension. If we let $t_2 = t_1 - \Delta t$ (so Δt is a positive quantity), and take the limit of $\Delta E_s/\Delta t$ as Δt goes to zero, we find

$$\frac{dE_s}{dt} = \frac{2\gamma HW}{t} \quad . \tag{2.4.2}$$

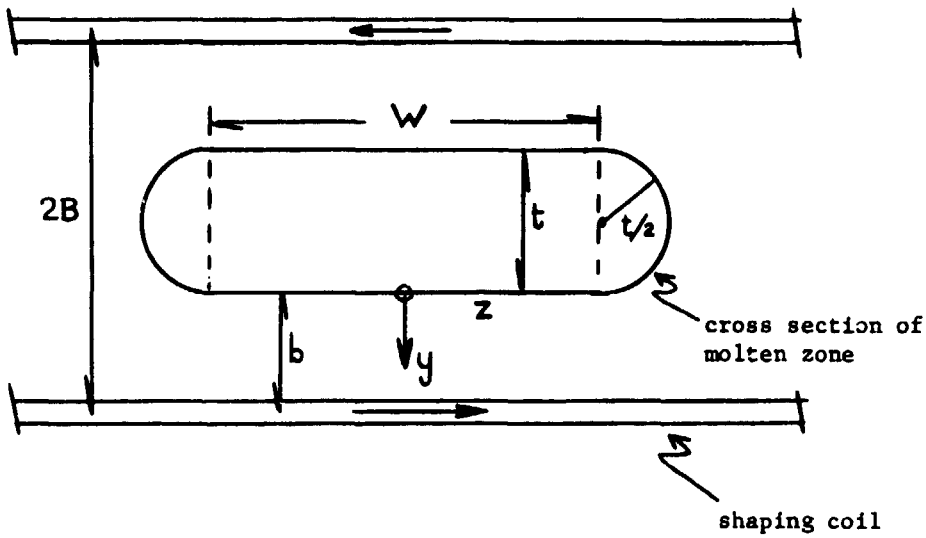

FIG. 2.4.1. ASSUMED CONFIGURATION AND NOMENCLATURE FOR DETERMINATION OF DEGREE OF SHAPING OF MOLTEN RIBBON BY HAIRPIN COIL

2.4.3 Electromagnetic Pressure

Although the eddy current force is a volume force, other discussions[1,2,11,14] have assumed it could be considered as a pressure at the surface of the melt. For purposes of comparison with the volume force equations which follow, we will discuss this approximation briefly. If p(t) is the electromagnetic pressure exerted when the ribbon thickness is t, the electromagnetic force on the shaping region is p(t)WH, neglecting the small total force on the semicircular regions. Then the work done on one half of the melt in compressing it from thickness t/2 to (t - Δt)/2 is $\bar{p}$WHΔt/2, where $\bar{p}$ is the average pressure exerted over the range Δt/2. (Also W is the average width, but we may ignore the weak dependence of W on t). If Δt is small, p is substantially constant between t and t - Δt, and the total electromagnetic work done on both faces is

$$\Delta Wk = pWH\Delta t \quad ,$$

or in the limit

$$\frac{dWk}{dt} = pWH \quad ,$$

If we imagine the ribbon being squeezed thinner and thinner by the field, the process will continue until the work required for an infinitesimal further reduction in thickness is just equal to that available, that is when

$$\frac{dE_s}{dt} + \frac{dWk}{dt} = 0 \quad . \tag{2.4.3}$$

If this occurs at a thickness of, say, t_f, then shaping stops when[1]

$$p(t_f) = \frac{2\gamma}{t_f} \quad . \tag{2.4.4}$$

2.4.4 Electromagnetic Work-Volume Forces

If we describe the situation in terms of f_n, the normal component of the volume force on the melt, then the pressure in the above equations is replaced by the integral of f_n--in particular,

$$\frac{dWk}{dt} = WH \int_{-\infty}^{0} f_n(y)dy \text{ (both faces)} \quad . \tag{2.4.5}$$

This formula was derived by Gaule' and Pastore[14]; we obtained it independently, but omit the proof. The lower limit on the integral should more properly be -t/2, but because of the rapid falloff of the force inside the melt, taking the limit to $-\infty$ is an excellent approximation as long as the ribbon is at least 3 or 4 skin-depths thick. Again, the small contribution from the semi-circular regions has been neglected.

2.4.5 Isolated Ribbon--Large β Approximation

To proceed, the integral in Eq. (2.4.5) must be evaluated. This can be readily done in the regime where the parameter β, the ratio of the distance of the wire from the melt to the skin depth, is large. The type of approximations required have been already discussed (Section 2.3); we only have to generalize slightly to obtain approximations valid for y not equal to zero. On the assumption that β is large enough that only the first terms of the asymptotic expansions contribute, we get from Eqs. (2.3.11) and (2.3.12), after expanding the square roots,

$$E_z(x,y) \approx \frac{-I}{\pi\sigma b\delta} \frac{1+i}{1+\xi^2} e^{\beta\eta(1+i)} \quad , \tag{2.4.6}$$

and

$$H_x(x,y) \approx \frac{I}{\pi b} \frac{1}{1+\xi^2} e^{\beta\eta(1+i)} \quad , \tag{2.4.7}$$

where we recall $\xi = x/b$ and $\eta = y/b$. Higher-order terms can be obtained if desired in terms of error functions of complex argument, but a more satisfactory procedure for obtaining the degree of shaping for moderate β's is described in the next subsection. Then since

$$f_n = \frac{\mu_0 \sigma}{2} \text{Re}\ (E_z\ H_x^*)$$

we find

$$f_n(\xi=0,y) = \frac{-\mu_0 I^2}{2\pi^2 b^2 \delta}\ e^{2\beta\eta} \quad , \tag{2.4.8a}$$

or

$$f_n(\xi=0,y) = f_{n0}\ e^{-2(|y/\delta|)} \quad , \tag{2.4.8b}$$

in an obvious notation. In agreement with our previous approximation we only need f_n for $\xi \approx 0$, so for the integral of Eq. (2.4.5) we obtain

$$\int_{-\infty}^{0} f_n\, dy = f_{n0}\, \delta/2 \quad .$$

Thus shaping may be considered to proceed until

$$\frac{2\gamma HW}{t_f} = \frac{WHf_{n0}\delta}{2} \quad , \tag{2.4.9}$$

or

$$\frac{2\gamma}{t_f} = \frac{\mu_0 I^2}{4\pi^2 b_f^2} \quad , \tag{2.4.10}$$

with the constraint $t_f + 2b_f = 2B$, where 2B is the distance across the shaping coil (Fig.2.4.1). Eq. (2.4.10) may be rewritten

$$t_f = K\ b_f^2 = K(B - \frac{t_f}{2})^2 \tag{2.4.11a}$$

where the parameter

$$K = \frac{8\pi^2\gamma}{\mu_0 I^2} \tag{2.4.11b}$$

has the dimensions of an inverse length. Inserting the value[8] appropriate to liquid silicon, $\gamma = 0.72$ N/m, we find

$$K = \frac{4.52 \times 10^7}{I^2} \quad m^{-1} \quad ,$$

where I is the peak coil current in amperes. Since t_f will be a fraction of a millimeter and since the rms current will commonly be given, we also write

$$K = \frac{2.25 \times 10^4}{(I_{rms})^2} \quad mm^{-1} \equiv \left(\frac{K_1}{I_{rms}}\right)^2 , \text{ say.}$$

where $K_1 = 150$ A/(mm)$^{1/2}$.

Eq. (2.4.11a) is readily solved for t_f:

$$t_f = 2B\left[\frac{1 + BK - \sqrt{1 + 2BK}}{BK}\right] \quad . \tag{2.4.12}$$

Alternatively, we can consider we know the ribbon thickness we want to obtain and solve for the current required to achieve it, given the size of the shaping coil:

$$I_{rms} = K_1 \frac{B - t_f/2}{t_f^{1/2}} = K_1 \frac{L}{t_f^{1/2}} \quad , \tag{2.4.13}$$

where the lengths B, b, and t_f are all to be expressed in millimeters. We repeat the conditions under which these equations can be used to predict the degree of shaping or current required:

1. $\beta = b/\delta$ should be large (say 5 or more).
2. δ must be considerably less than t (say no more than t/3).

These requirements may be met by operating at a high enough frequency; we shall see in the following section that total power required increases gradually with frequency, but even at the lowest frequencies liable to be used, the approximations are likely to be satisfactory in any practical situation. It should be noticed that in this regime the current (though not the power) required for shaping to a given thickness is independent of the skin depth, and thus of the operating frequency.

To provide some numerical examples, if one wants a ribbon 0.4 mm thick, then if b is about 2.8 mm, as in the smallest coil discussed in Reference 1, the rms current required is around 660 A, while if the wires can be brought in so that b is only .25 mm, the current required is 59 A. Clearly the trade-off of greatest importance is that between getting the wire close enough to get the current down and having it large enough to carry the current without melting. (Note that b is the distance from the melt to the center of the wire). Of course if the wire comes extremely close to the melt, the presence of the eddy currents will affect the current distribution in the wire; we will not pursue this extremely complicated problem, but just point out that Lenz's Law shows that this effect will reduce the force on the melt, and that a somewhat higher current will be required for a given ribbon thickness than would be expected on the basis of the theory presented here. A sharp-pointed concentrator[14] may be a good way to get the current close to the melt; it will still clearly have to reach at least as close as the distance b, though.

The work of Gaule' and Pastore[14] has been used[2] to estimate power and current requirements for electromagnetic shaping. Their approach and assumed physical situation are rather different from ours, but a comparison insofar as is possible shows the following:

1. They do not discuss the distance of the coil from the melt, and because of the nature of their approximations apparently did not realize the importance of this parameter.
2. They assume $H_x(0,0) = \frac{2I}{t}$, and $\delta = t/4$. From Eq. (2.4.7), we see $H_x(0,0) = \frac{I}{\pi b}$. By comparing these equations, we see that their assumptions amount to taking $\beta = 2/\pi$. But otherwise their equations are similar to those based on the asymptotic expansions discussed above. Thus it appears that they are using asymptotic formulas in a region (β not $\gg 1$) where they do not apply.
3. The fact that they considered Ge, with a surface tension about 0.6 N/m, rather than Si; a factor of 2 error in their equation for the pressure; and their other approximations enabled Gaule' and Pastore to find the rather small value of 12 A required for shaping to .3 mm thickness.

2.4.6 Isolated Ribbon--Arbitrary β

By evaluating an integral numerically, we may extent the results of the previous section to smaller β's and determine the range of validity of the asymptotic approximation used there.

Eq. (2.4.5) may be rewritten

$$\frac{dWk}{dt} = \frac{WH\mu_0\sigma}{2} \operatorname{Re} \int_{-\infty}^{0} E_z(0,y)H_x^*(0,y)dy \quad . \tag{2.4.5'}$$

Introducing the integral expressions (eqs. (2.3.11) and (2.3.12)) for E_z and H_x, we may write this as

$$\frac{dWk}{dt} = \frac{WH\sigma\omega}{2} \left(\frac{\mu_0 I}{\pi}\right)^2 \operatorname{Im} \int_{-\infty}^{0} dy\, I_1 I_2 \quad , \tag{2.4.14a}$$

where

$$I_1 = \int_0^{\infty} \frac{dk\, e^{-kb + \sqrt{k^2+\alpha^2}\, y}}{k + \sqrt{k^2+\alpha^2}} \quad , \tag{2.4.14b}$$

and

$$I_2 = \int_0^{\infty} \frac{dq\, e^{-qb + \sqrt{q^2-\alpha^2}\, y}\, \sqrt{q^2-\alpha^2}}{q + \sqrt{q^2-\alpha^2}} \quad . \tag{2.4.14c}$$

Changing variables of this triple integral to $\eta = y/b$, $u = \delta k$ and $v = \delta q$, and doing the η integral, which is a simple exponential, we find

$$\frac{dWk}{dt} = \frac{-HW\mu_0 I^2}{4\pi^2\delta^2} F(\beta) \quad , \tag{2.4.15a}$$

where

$$F(\beta) = \int_0^{\infty}\int_0^{\infty} du\, dv\, e^{-\beta(u+v)} \operatorname{Im} f(u,v) \quad , \tag{2.4.15b}$$

and

$$f(u,v) = \frac{-4\sqrt{v^2-2i}}{(u+\sqrt{u^2+2i})(v+\sqrt{v^2-2i})\,(\sqrt{u^2+2i}+\sqrt{v^2-2i})} \quad . \tag{2.4.15c}$$

The quantity f(u,v) can, if desired, be separated algebraically into its real and imaginary parts, but it is easier and faster computationally to let the computer take care of this. The function Im f(u,v) varies smoothly and is generally well-behaved in the first quadrant of the u,v-plane. It has a value of unity at the origin and falls smoothly with finite slope in all directions from there. The function becomes slightly negative near the u-axis for u greater than about 0.75, but this introduces no difficulty in evaluation of the integral. It is simpler for comparison with previous calculations to change variables again to $s = \beta u$ and $t = \beta v$; then

$$\frac{dWk}{dt} = \frac{-H\omega\mu_0 I^2}{4\pi^2 b^2} G(\beta) \quad , \tag{2.4.16a}$$

$$G(\beta) = \int_0^\infty \int_0^\infty ds\, dt\, e^{-(s+t)} \mathrm{Im}\, f(s/\beta, t/\beta) \quad , \tag{2.4.16b}$$

with f as given above. Comparison with Eqs. (2.4.5) and (2.4.9) shows our previous asymptotic approximation amounts to taking $G(\beta) = 1$, independent of β.

Since the integrand of (2.4.16b) is in the form of a double Laplace transform, it seems natural to try to evaluate by means of a product Gauss-Laguerre numerical integration routine[21]. Such a routine was written and used to evaluate $G(\beta)$ in the range $0.5 \le \beta \le 44$. Fig. 2.4.2 shows results for β between 0.5 and 6. At $\beta = 44$, $G(\beta) = 0.9770$. The evaluation used the first 16 x 16 points of a 28 x 28 Gauss-Laguerre scheme. (Because of the generally decreasing nature of the integrand, points further from the origin do not contribute appreciably to the integral, and it is a waste of time to evaluate them). The accuracy of the integration routine was tested by trying some integrands which could be integrated numerically, and also by redoing the integral of interest here for several β's by 16 x 16 point Gauss-Legendre quadrature in 36 or 81 subintervals. In the latter procedure, appropriate upper-limit cutoffs to the integral must be introduced; there is no problem in doing this so that the remainder is negligible. It was found that the simple Gauss-Laguerre procedure could be relied on to 5 decimal places for

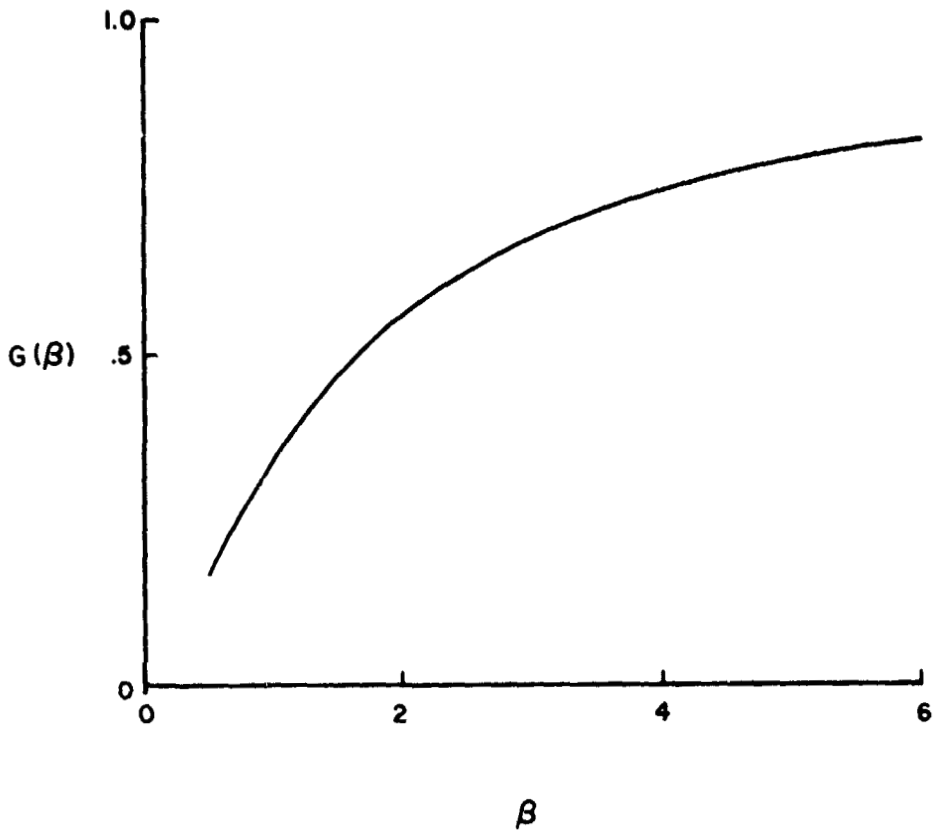

FIG. 2.4.2. THE FUNCTION G(β) DEFINED BY EQS (2.4.16b) AND (2.4.15c)

$\beta \geq 2.5$, and gave an error in $G(\beta)$ of only 0.77 percent for $\beta = 0.5$. The error as a function of β is graphed in Fig. 2.4.3. The value returned by the Gauss-Laguerre quadrature program is invariably slightly higher than the true value. The quadrature scheme will be rather inaccurate for very small β's, but the small β region is not of much physical interest.

It is apparent that the asymptotic approximation is not very accurate for β's in the range discussed earlier. For the problem of shaping at constant volume discussed there, all that needs to be done to make the theory correct for any β is to replace b_f in Eq. (2.4.10) by $b_f/(G(\beta))^{1/2}$. Thus, the current required to achieve a given degree of shaping will be a factor $(G(\beta))^{-1/2}$ larger than would be calculated from the asymptotic expansion. For $\beta = 2/\pi$, the current required for shaping to a given thickness is 2.1 times larger than the asymptotic value.

2.4.7 Degree of Shaping in RMGS Configuration

In a recent study[2] at McDonnell-Douglas of potentialities for space manufacture of Si, a technique termed Ribbon from Melt Growth in Space, or RMGS, has been described. It is discussed briefly elsewhere in the report; the salient idea as far as the present discussion is concerned is that the ribbon is drawn through the shaper from a freely floating sphere of molten Si. The constraint of constant cross-section then no longer operates; one may look at the process as one in which the excess Si is squeezed back into the sphere when the coil current is turned up to thin the ribbon. Since the sphere radius is large, one might anticipate that the free energy change on shaping would be less than that calculated previously. We wish to assess the effect of this change in configuration on the degree of shaping for a given coil current.

An analysis[11] has recently been made by R. Rochat of McDonnell-Douglas of the expected shape of the meniscus from the ribbon to the sphere and of shaping pressure, assumed applied uniformly over a height H, required to shape the ribbon to a given final thickness. Numerical methods were required for this analysis and the results have been presented graphically.

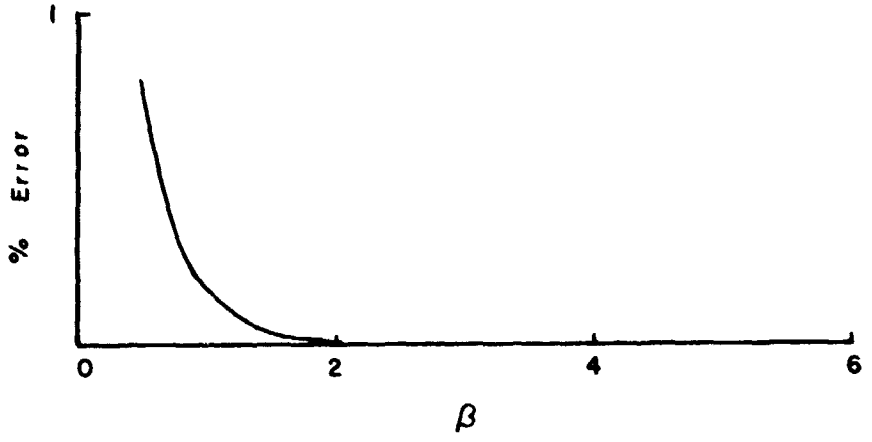

FIG. 2.4.3. ERROR IN CALCULATION OF $G(\beta)$ BY 16 x 16 ORDER PRODUCT GAUSS-LAGUERRE QUADRATURE

We have not had an opportunity to check this work independently, but find no reason to doubt its correctness. The effects of the curvature at the edge of the ribbon have not been included, but this may not be a severe approximation in these circumstances. One parameter entering the calculation is the ratio of the height of the region being shaped to the total vertical height of the meniscus region. The present discussion will be most appropriate when this ratio is not too large--say 1/2 or less; however, the results of the surface stress analysis do not depend strongly on this parameter.

The principal result of the analysis is that the shaping pressure is given, instead of by Eq. (2.4.4), by

$$p = \gamma f/H \quad , \tag{2.4.17}$$

where f is a dimensionless function* of the ribbon thickness t, the sphere radius R_s, the ratio N discussed above, and H. The principal properties of the function f for our purposes are

1. f is always greater than one.
2. for any reasonable set of parameters, the value of $\sqrt{f}$, which we will see to be the parameter of greatest interest, will lie between 1 and 2. Generally it will be rather close to 1.

From Eqs. (2.4.3), 2.4.16) and (2.4.17), we find the peak current required for shaping to thickness t under these circumstances is given by

$$I_{RMGS} = 2\pi b \left(\frac{\gamma f}{\mu_0 HG(\beta)}\right)^{1/2} \quad . \tag{2.4.18}$$

It is interesting to compare this to the current required for shaping of an isolated ribbon, I_R, which can be found from Eqs. (2.4.2), (2.4.3) and (2.4.16). We obtain

$$\frac{I_{RMGS}}{I_R} = \left(\frac{t}{2H}\,\frac{f}{G}\right)^{1/2} \quad . \tag{2..19}$$

---

* Elsewhere in the report, f denotes frequency. This dimensionless function f will only be used in this subsection.

f/G will be greater than unity. t/2H might be small, but if H is large so are b and, consequently, I_R. To pursue this further, we need a specific relationship between H, the height effectively shaped, and b, the distance of the wire from the melt. A reasonable approximation may be obtained by averaging the normal force, given by Eq. (2.3.32) for large β's, over ξ, the normalized distance along the ribbon. One obtains

$$H = \frac{\pi}{2} b \Gamma(\beta) \quad , \tag{2.4.20a}$$

where

$$\Gamma(\beta) = 1 - \frac{1}{2\beta} + \frac{1}{8\beta^2} \quad . \tag{2.4.20b}$$

Now let us specialize to the case we have frequently discussed, where $\delta = t/4$. (One can readily generalize to other ratios; this is discussed qualitatively below). Then we can express the current ratio almost completely (except for $\sqrt{f}$) in terms of the dimensionless parameter β:

$$\frac{I_{RMGS}}{I_R} = \Phi(\beta) \sqrt{f} \quad , \tag{2.4.21a}$$

where

$$\Phi(\beta) = (4/\pi\beta\Gamma G)^{1/2} \quad . \tag{2.4.21b}$$

$\Phi(\beta)$ is plotted in Fig. 2.4.4. We see that for small enough β--β less than 2.5 for $\sqrt{f} \approx 1$--the ratio I_{RMGS}/I_R will be greater than unity; so for small β it will be more difficult to shape the ribbon when it is attached to the spherical melt. For larger β's, though, there will be a diminution of current required for shaping to a given thickness from a given distance when the presence of the spherical melt is considered.

I_R will also depend on β of course; so more current will be required when b is larger. Again assuming $t/\delta = 4$, we can write

$$I_R = \pi\beta \, (2\delta\gamma/\mu_0)^{1/2};$$

so

$$I_{RMGS} = \pi \, (2\delta\gamma/\mu_0)^{1/2} \, \beta \, \Phi(\beta) \sqrt{f} \quad . \tag{2.4.22}$$

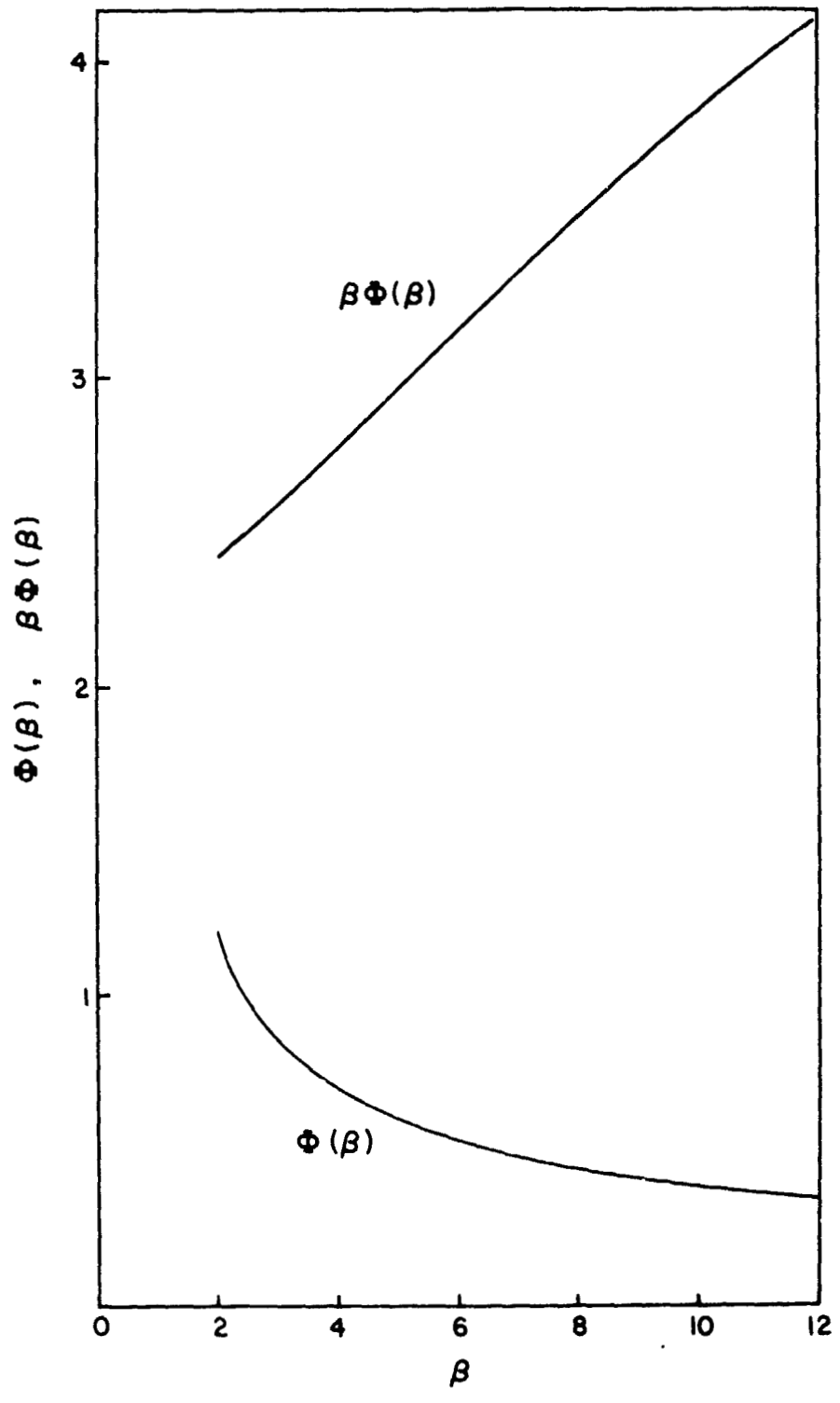

FIG. 2.4.4. THE FUNCTION $\varphi(\beta)$ OF EQ. (2.4.21b), AND $\beta\varphi(\beta)$

$\beta\ \Phi\ (\beta)$ is also plotted in Fig. 2.4.4 and is seen to increase slowly with β. Thus the advantage to be gained by bringing the wire in close to the melt is not extremely large; on the other hand, the penalty for moving the wire further away is not so great. To give a specific numerical example, suppose $\delta = 100\ \mu m$. Then the rms current required for shaping a 400 μm ribbon is given by

$$I_{RMGS}^{rms} = 23.8\ \beta\ \Phi(\beta)\ \sqrt{f}\ A \quad . \tag{2.4.23}$$

Taking $\sqrt{f} = 1.03$ as a not untypical value, we find the current required for various distances from the shaper to the melt as in the following table:

TABLE II. rms CURRENT AT 21 MHz REQUIRED TO SHAPE Si RIBBON TO 400 μm THICKNESS

Shaper-to melt distance, b(μm)	rms current (A)
200	59
500	73
1000	95
1200	102

If we had assumed a ratio $t/\delta = \tau$, say, instead of 4, we would obtain a factor of $(4/\tau)^{1/2}$ on the right side of (2.4.23). Thus some saving in current required can be obtained by reducing δ. But the only way to do this is to increase the operating frequency. Since $\delta \propto \omega^{-1/2}$, $I \propto \omega^{-1/4}$; so the frequency must be increased by a factor of 16, to over 330 MHz in the situation described above, to cut the current required by half.* The ac resistance of both the shaper coil and the melt will also increase with ω; the combined effects of all these changes are discussed in Section 2.5.

* or less, if the frequency dependence of $\beta\ \Phi\ (\beta)$ is considered.

2.4.8 Degree of Flatness

We have assumed to this point that the ribbon was essentially flat, its cross section at the plane of the shaper being a rectangle terminated by two semicircles as in Fig. 2.4.1. While the physical situation surely indicates that the ribbon will be fairly flat, it would be useful to have some measure of what the departure from flatness might be. In this section, we estimate this quantity for the case of large β where the departure from flatness is most likely to be significant. To make such an estimate, we have to make some assumption as to the shape of the ribbon cross section, since we do not know what the shape of lowest total energy will be. We will take the cross section to be an ellipse of the same area as the flat ribbon. Then by trying ellipses of different eccentricities, we can determine the elliptical shape of least total energy, which should be good approximation to the actual shape taken up by the ribbon at the plane of the shaper.

The geometry of the situation is illustrated in Fig. 2.4.5. The equation of the melt surface is

$$\frac{y^2}{p^2} + \frac{z^2}{q^2} = 1 \quad ,$$

where the area of the cross section is

$$A = \pi\, pq = Wt + \pi t^2/4 \quad .$$

Since A is fixed, if we select a trial value for the semi-minor axis p (presumably a little more than t/2), q is determined; so there is just one free parameter to vary.

Again assuming the shaping takes place uniformly over a height H, the change in surface energy on going from the flat to the elliptical cross section is

$$\Delta E_s = \gamma H[4q\, E(\sqrt{q^2 - p^2}/q) - (2W + \pi t)] \quad , \qquad (2.4.24)$$

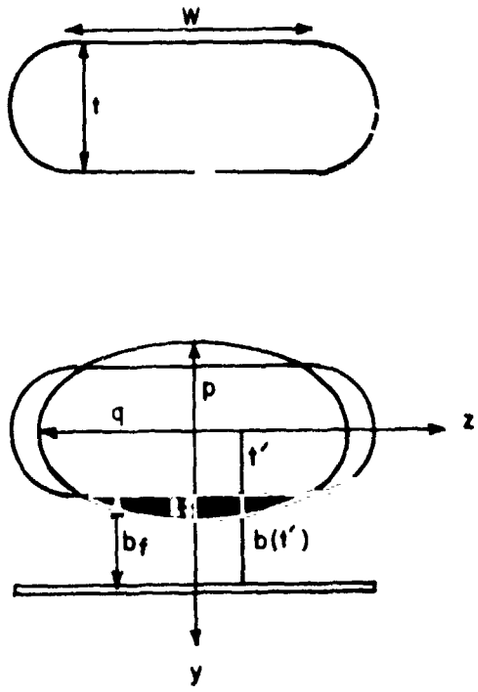

FIG. 2.4.3. DEFORMATION OF FLAT RIBBON OF WIDTH W, THICKNESS t, INTO RIBBON OF ELLIPTICAL CROSS SECTION WITH SEMIAXES p and q

where E denotes a complete elliptic integral[22]. The corresponding change in electromagnetic energy may be approximated by assuming that each small element Δz of the melt is part of a very wide flat plate of thickness $t(z)$ and distance $b(t)$ from the shaper. Since the shape of the melt only changes gradually, this should be a good approximation. Then the change in electromagnetic energy on going from the flat to the elliptical configuration is obtained by calculating the energy change for each region of width Δz using Eqs. (2.4.5) and (2.4.8), and summing over all the strips from $z = -W/2$ to $z = +W/2$. For consistency with the previous approximations we again neglect, if possible, the electromagnetic forces on the very edges of the ribbon. Thus we have

$$\Delta Wk = 2H\,[\mu_0 I^2/4\pi^2]\int_0^u dz \int_{t/2}^{y(z)} dt'\,[b(t')]^2 \quad , \tag{2.4.25}$$

where

$$u = \min\,[W/2,\ q] \quad .$$

The current I is fixed at the value that was calculated necessary to shape a flat ribbon of thickness t, so it is given by Eq. (2.4.10):

$$\mu_0 I^2/4\pi^2 = 2\gamma b_f^2/t \quad ,$$

where b_f denotes the value of b for a flat ribbon. What we want to do is to calculate the total energy change $\Delta E_{total} = \Delta E_s + \Delta Wk$ as a function of the amount of "bulge" in the ribbon (ℓ in Fig. 2.4.5), and the other parameters, and to see whether there is some value of ℓ for which the energy change is a minimum and negative--if there is, a configuration similar to that elliptical one will probably be taken up by the ribbon. The integrals in Eq. (2.4.25) can be done analytically, but since the results are rather complicated, we shall just present some results graphically. It will be convenient to divide both ΔE_s and ΔWk by the factor $(2\gamma WH/\pi)$, and to compare the dimensionless quantities resulting. If we also take as a dimensionless independent variable the fractional bulge at the ribbon center* $\alpha = 2\ell/t$, we find there are only

* This α should not be confused with the α that was used in section 2.3

two dimensionless parameters in the problem:

1. $s = \pi t/4W$, a quantity depending on the aspect of the flat ribbon. Both ΔE_s and ΔW_k depend only very weakly on this parameter, but we will assume a large but finite aspect ratio, $W/t = 150$, for purposes of calculation.
2. $r = 2b_f/t$, a measure of the relative size of the shaping coil. ΔE_s of course is independent of this parameter. For our usual assumed conditions, where $t = 4\delta$, r is related to our usual parameter β by $r = \beta/2$.

Some calculated results are shown in Fig. 2.4.6. It appears that although there is no small change from flat ribbon for which the departure results in a decreased total energy, this is primarily because a large bulge is necessary for the surface energy to decrease, and it does appear that for some increase in thickness in excess of 30 percent, an elliptical cross section will be more stable. We have not made calculations to determine the minimum energy configuration for this region though, since with further increases in thickness, we are getting rapdily into the region where the asymptotic approximation breaks down. Even if more elaborate calculations (which could be carried out numerically) showed that the total energy change was never quite negative, but only reached a minimum, the presence of such a low-energy configuration could be important in determining the stability of the system against vibrations or other mechanical perturbations. Finally, we wish to re-emphasize that there are liable to be changes in ribbon shape between the shaper plane and the level of the freeze, which we have not considered in this section.

2.5 Power Requirements

In this section we estimate the total power needed for shaping to a specified thickness, with a coil of given dimensions, in both the isolated ribbon and RMGS situations.

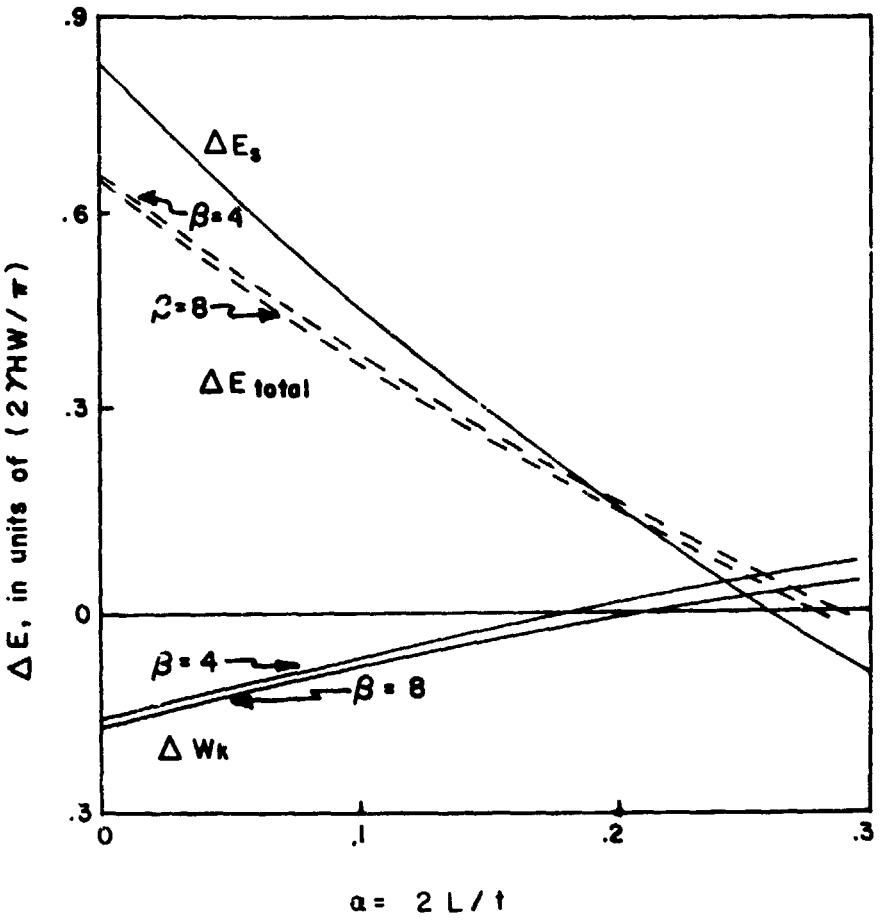

FIG. 2.4.6. CHANGE IN ELECTROMAGNETIC, SURFACE, AND TOTAL ENERGY WITH RELATIVE ELLIPTICAL DISTORTION OF MELT

The total steady power P_t needed at the input to the shaper coil will be the sum of the power dissipated in the melt, P_m, and that dissipated in the coil, P_c. The power dissipated in the melt is given by the real part of the integral of the Poynting vector over the ribbon surface, Eq. (2.2.13). In the asymptotic (large β) regime, we find, using just the first terms of (2.3.20) and (2.3.21),

$$P_m = \mu_o I_{rms}^2 f W \beta^{-1} \quad , \tag{2.5.1}$$

where we recall W is the ribbon width and f is the operating frequency. Use of the asymptotic values for the fields is not as severe an approximation as it was for determining degree of shaping, and (2.5.1) will be correct to within 10 percent at $\beta = 5$ and more accurate for larger β's.

If we take the coil to have a circular cross section of radius a, then the power dissipated in the coil is given by[23]

$$P_c = I_{rms}^2 R_{ac} \quad , \tag{2.5.2a}$$

where

$$R_{ac} = (a/2\delta_c) R_{dc} \quad , \tag{2.5.2b}$$

$$R_{dc} = (\rho_c L/\pi a^2) \quad , \tag{2.5.2c}$$

where ρ_c is the resistivity of the coil material and L is the total length of the coil. δ_c is the skin depth in the coil, determined by ρ_c and the operating frequency, and we have made the generally very good assumption that $a \gg \delta_c$. The power dissipated in the coil will frequently be comparable to that dissipated in the melt so it must be included in any realistic estimate.

Adding (2.5.1) and (2.5.2), we obtain

$$P_t = \mu_0 I_{rms}^2 f \delta \left[\frac{W}{b} + \frac{L}{2a} \frac{\delta_c}{\delta} \right] \quad . \tag{2.5.3}$$

Inserting the value of the current obtained from Eq. (2.4.10), we find for the <u>isolated ribbon</u>

$$P_t^{IR} = 4\pi^2 \gamma f \delta b^2 t^{-1} \left[\frac{W}{b} + \frac{L}{2a} \frac{\delta_c}{\delta} \right] \quad . \tag{2.5.4}$$

In this form it is clear that $P_t \propto f^{1/2}$, or $P_t \propto \delta^{-1/2}$. Thus for a specified ribbon thickness and coil dimension, the power required may be reduced somewhat by running at a larger skin depth. Of course with too large a skin depth the normal shaping force on one face of the ribbon will be reduced by the force coming through from the other side, and the shaping effect will be reduced. Presumably the optimum δ for given conditions could be established by a numerical procedure such as that described in Section 2.6. Furthermore, we can see from the discussion of Section 2.4.6 that the current required will increase somewhat with decrease in frequency. Selection of suitable operating voltage and frequency cannot therefore be made quite independently.

The necessity of avoiding contact between the ribbon and the shaper will doubtless lead to some minimum clearance that can be allowed between the shaper and the melt. While this will naturally depend on the other parameters of the problem, let us assume that it can be taken as an independent design variable and call it c. Thus c = b-a. In the isolated ribbon situation, it is easy to show that there is an optimum value of the ratio c/b for which the power required is minimum. If we assume, as in some of the McDonnell-Douglas calculations, that L = 3W, and further assume that the coil is copper, of resistivity 1.7×10^{-8} ohm m, then the optimum value of c/b is 0.704, and roughly 40% of the power is dissipated in the coil and 60% in the melt. If we assume our usual operating conditions f = 21.1 MHz, t = 400 μm, W = 6 cm, then the total power required is simply given by

$$P_t^{IR}(\text{kW}) = 22.06\ c \quad , \tag{2 5.5}$$

where the clearance c is in millimeters. For any reasonable value of c, this is quite a substantial power requirement, enough to make electromagnetic shaping of an isolated ribbon relatively unattractive.

In the RMGS situation, if we take as unity the function f discussed in Section 2.4.7, we have

$$P_t^{RMGS} = P_t^{IR}[\Phi(\beta)]^2 \quad , \tag{2.5.6}$$

where $\Phi(\beta)$ was given by (2.4.21b) and we must remember that we have already specialized to the case $\delta = t/4$. In this case we find that rather than

there being an optimum c/b, for fixed c the power required approaches a minimum as $b \to \infty$. Explicitly,

$$P_t^{RMGS}(\min) = 4\pi\gamma f W J (1+(L/2W)(\delta_c/\delta)) \quad . \tag{2.5.7}$$

For the same conditions as used above for the isolated ribbon, we find that this minimum power is only $P_t^{RMGS}(\min) \approx 1.4$ kW. Of course the actual power required will be more than this, since b cannot be too large for the current to be reasonable--a few values are given in Table III--; but in any event the total power requirement in these circumstances seems quite moderate, and much less than for the isolated ribbon in similar circumstances. Thus although the current required in the RMGS configuration is higher than that which might be expected from naive considerations, the power requirements are such that the process appears from this standpoint rather attractive. Of course the interaction with the meniscus region, which would certainly increase the power required, has not been included. A realistic calculation of this effect appears extraordinarily difficult, though.

TABLE III. POWER (IN kW) REQUIRED FOR SHAPING RMGS CONFIGURATION AS FUNCTION OF DISTANCE b FROM MELT SURFACE TO CENTER OF SHAPER AND OF CLEARANCE c BETWEEN SHAPER AND MELT.

b (mm) \ c (mm)	0.25	0.5	1.0	1.5	2.0
.8	1.84	2.20			
1.2	1.66	1.79	2.99		
1.6	1.59	1.66	1.99	5.61	
2.0	1.54	1.59	1.77	2.30	
2.4	1.51	1.55	1.67	1.92	2.80
2.8	1.50	1.53	1.62	1.77	2.12

2.6 Effects of Freezing Interface and of Finite Ribbon Thickness

It will be shown in Section 2.7 that the liquid-solid interface will typically be well away from the shaping region; thus treating this region as all liquid silicon will generally be a very good approximation. It is possible, though, that the interface might be brought closer to the shaping level by some auxiliary cooling method, and it would be of interest to know quantitatively what changes the presence of the solid region would make to the fields, forces, degree of shaping, etc. In this section, we outline a numerical procedure which would enable one to determine the electric field distribution in the situation described. From this, the magnetic field, forces, etc., can be estimated by standard numerical techniques. If there is negligible time delay in the shaping coil, a strict boundary condition at the center plane of the ribbon (solid or liquid) is that the electric field be zero. By adopting this boundary condition, we are also enabled to investigate effects resulting from the ribbon being thinner than a few skin depths (though at least one skin depth thick) by such a numerical technique. While computer subroutines have been written to handle most aspects of the numerical procedures involved, lack of time at the conclusion of the program has prevented us from running these programs to any great extent.

The method adopted is a modification of one due to Stoll.[24] This method is essentially one of finite-difference approximation to the scalar Helmholtz equations for the complex electric field. Stoll has ingenuously modified this equation, however, to take the magnetic field boundary conditions into account, by assuming a smoothed spatial variation of the magnetic permeability. The method is applicable to fields which depend on two dimensions only and to regions with rectangular boundaries. Extension to more general regions might be possible, but would be quite difficult. On the other hand, the method is readily applied to any number of subregions of different materials and to any number of current sources, either distributed or infinitesimal.

To solve the Helmholtz equations by a finite-difference method, it is necessary to fix the field on some suitable boundary of the region within which a mesh of sample points is to be defined. In the problems discussed by Stoll,[24] it is possible to choose a boundary on which the electric field is negligibly small, and may be taken to be zero. Even in these cases, many points outside

the eddy current region must be included in the mesh, though. In ou situation, where there is a current source in the vacuum region outside the melt, including enough points in the vacuum region that the field be negligible is out of the question. We can, however, find a boundary in the vacuum region where the real part of the field is negligible and the imaginary part is close to that of the problem previously solved with the ribbon assumed thick and entirely liquid. Thus by having solved the previous problem, we can obtain a suitable starting point from which we can bootstrap our way to a solution in the present more complex case.

It is possible again, as in Sec. 2.3, to normalize all distances to b, the distance of the shaping wire from the melt. Thus the only parameters entering the problem are β, the ratio of the shaper distance b to the skin depth in the liquid δ; $\xi_0 = x_0/b$, the relative distance to the solid-liquid interface from the shaping plane; $P = \rho/\rho_s$, the ratio of the resistivities in the liquid and the solid, and the exciting current I. We will see that the numerical procedure will only be reliable, with a mesh of reasonable size, for rather large β's--say $\beta \geq 10$. The setup of the region over which the finite-difference mesh is to be described is shown in Fig. 2.6.1. We recall that $\xi = x/b$ and $\eta = y/b$. By consideration of our previous results and of numerical results on simpler problems,[24] we judge that a mesh size of $\Delta\xi = .2$ and $\Delta\eta = .2\beta^{-1}$ in the liquid and solid, $\Delta\eta = .2$ in the vacuum out to $\eta = 4$, and $\Delta\eta = 1$ for $\eta > 4$ should be sufficient to determine the fields to within a few percent. A portion of this mesh is also shown in Fig. 2.6.1.

From Eqs. (2.3.3c) and (2.3.10a), we can show, using the identity[16]

$$k^{-1}(k^2 + \alpha^2)^{1/2}/(k + (k^2 + \alpha^2)^{1/2}) = k^{-1} - (k + (k^2 + \alpha^2)^{1/2}) \quad , \quad (2.6.1)$$

that the unperturbed electric field in the vacuum region is given, for large β, by

$$E_v = \frac{-i\mu_0\omega I}{2\pi} \left\{ 1/2 \ln \frac{\xi^2 + (\eta+1)^2}{\xi^2 + (\eta-1)^2} + \chi(u,v) \right\} \quad , \quad (2.6.2)$$

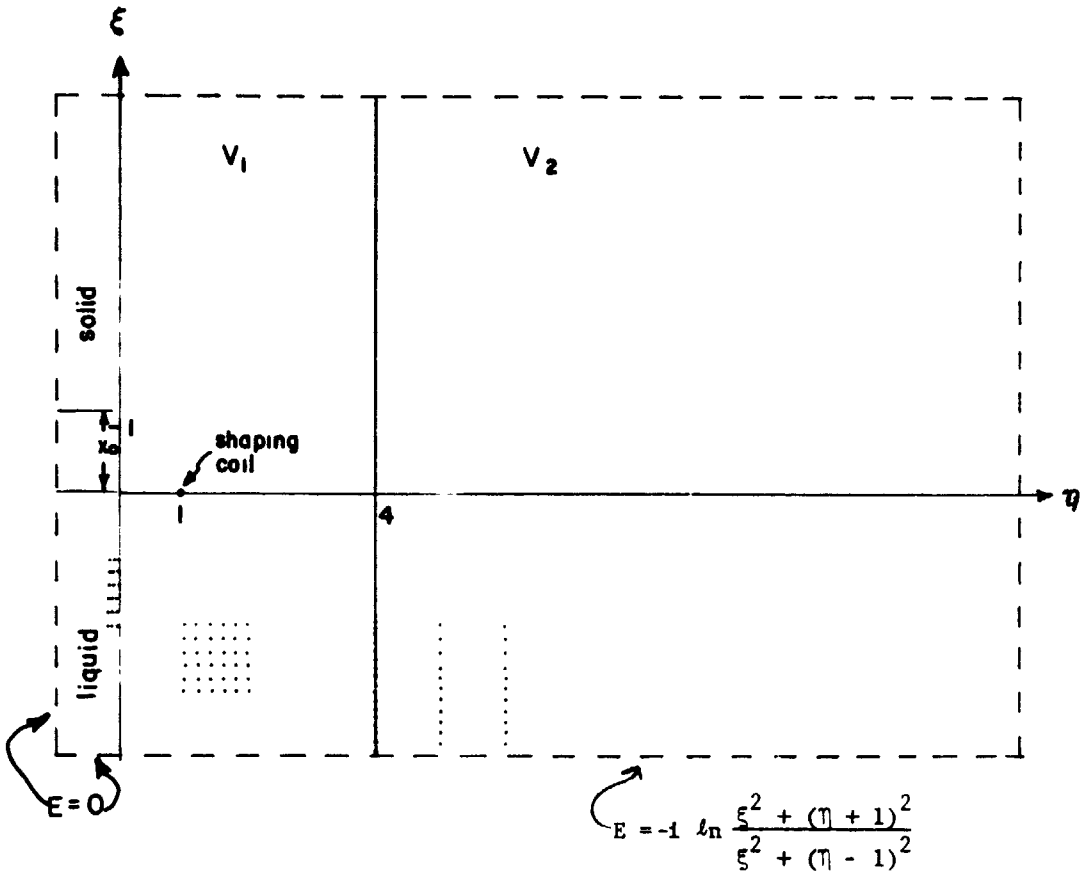

FIG. 2.6.1. FINITE-DIFFERENCE GRID IN NORMALIZED COORDINATES FOR NUMERICAL SOLUTION OF A TWO-DIMENSIONAL EDDY-CURRENT PROBLEM

where

$$u = \beta(\eta+1), \quad v = (\xi/(\eta+1))^2, \text{ and}$$

$$\chi(u,v) = u^{-1}\left[\frac{1-i}{1+v} + \frac{i}{u}\frac{1-v}{(1+v^2)2} - \frac{1+i}{2u}\frac{1-3v}{(1+v^2)3} + \cdots\right].$$

By evaluating this expression for large β's and by numerical calculation of an integral for χ in a way similar to that of Sec. 2.4.6, we found, for instance, that for $\beta \geq 10$: 1) the real part of χ would be no more than 7% of the magnitude of the field at the origin at $\eta = 14$, 2) the imaginary part of χ would be more than one order of magnitude smaller than the real part, and 3) Re χ is no more than 5% of the logarithmic term. The situation would of course be improved if we took the skin depth as that of the solid. Thus if we take $\eta = 14$ as the right-hand boundary of the sample region, and fix the electric field there as that due to the logarithmic term (which will be the same regardless of ξ_0), we might anticipate reasonably accurate results (though possibly 5 to 10% off) in the region of interest near the ribbon surface. A similar analysis along the ribbon-vacuum interface (where the logarithmic term is zero) indicates that even for $\xi_0 = 0$, similar accuracy could be obtained by going from $\xi = -4$ to $\xi = +6$, again fixing E along these lines as the value of the logarithmic term. Interior to the ribbon, it will be satisfactory to take E = 0 on the horizontal boundaries as well as at the ribbon mid-plane. With the mesh described above, there are 1911 interior points at which the field must be determined if these limits on ξ and η are adopted. Of course it is prudent to make the limits variable in computer programming in order to allow for possible poor convergence or for future refinement, but the amount of computer time and memory required mount rapidly.

By hypothesis the exciting current wire (which we shall take to be of infinitesimal size) lies on a mesh point. Since the mesh points are closely spaced, it will be satisfactory to assume that the interface plane $\xi = \xi_0$ passes through a row of mesh points. One parameter of the problem is eliminated

if we define all fields in terms of a reference field $E_R = \rho I/(2\pi\delta^2)$. Then the field at a given mesh point E_0 is given in terms of fields at adjoining mesh points E_1-E_4 (Fig. 2.6.2), for each of the regions of Fig. 2.6.1, by the following equations:

in region v_2,

$$E_0 = (E_1+E_3+25(E_2+E_4))/52 \quad ; \tag{2.6.3}$$

on the v_2-v_1 boundary,

$$E_0 = (E_1+5E_3+15(E_2+E_4))/36 \quad ; \tag{2.6.4}$$

in region v_1

$$E_0 = (E_1+E_2+E_3+E_4-i\pi\delta(\xi)\delta(\eta-1))/4 \quad ; \tag{2.6.5}$$

in the liquid,

$$E_0 = \frac{\beta^2(E_1+E_3)+E_2+E_4}{2\ (1+\beta^2+i\beta^2/25)} \quad ; \tag{2.6.6}$$

in the solid,

$$E_0 = \frac{\beta^2(E_1+E_3)+E_2+E_4}{2\ (1+\beta^2\ \ \beta^2P/25)} \quad ; \tag{2.6.7}$$

on the liquid-vacuum boundary,

$$E_0 = \frac{2\beta E_1+2\beta^2E_3+(1+\beta)(E_2+E_4)}{2\ ((1+\beta)^2+i\beta^2/25)} \quad ; \tag{2.6.8}$$

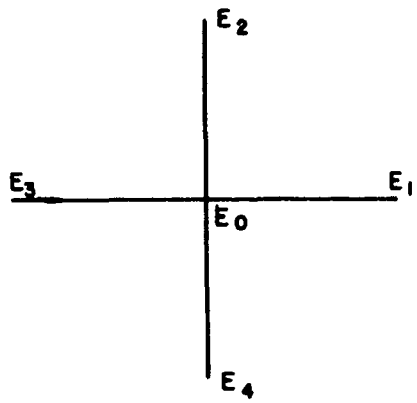

FIG. 2.6.2. NOTATION FOR MESH POINTS ADJOINING A GIVEN MESH POINT

on the solid-vacuum boundary,

$$E_0 = \frac{2\beta E_1+2\beta^2 E_3+(1+\beta)(E_2+E_4)}{2\,((1+\beta)^2+i\beta^2 P/25)} \quad ; \tag{2.6.9}$$

on the solid-liquid boundary,

$$E_0 = \frac{\beta^2(E_1+E_3)+E_2+E_4}{2\,(1+\beta^2)+i(1+P)\beta^2/25} \tag{2.6.10}$$

and at the point where solid, liquid and vacuum meet,

$$E_0 = \frac{2\beta E_1+2\beta^2 E_3+(1+\beta)(E_2+E_4)}{2\,(1+\beta)^2+i(1+P)P^2/25} \quad ; \tag{2.6.11}$$

together with the conditions at the points on the boundary:

$$E = -i\,\ln\frac{\xi^2+(\eta+1)^2}{\xi^2+(\eta-1)^2} \tag{2.6.12}$$

on the external boundary; and

$$E = 0 \tag{2.6.13}$$

on the boundary inside the ribbon. In (2.6.5), the deltas are defined by $\delta(x) = 1$ if $x = 0$, $\delta(x) = 0$ otherwise.

There are a number of ways of looking at the problem of solving the very large set of coupled equations represented by (2.6.3) - (2.6.13). One might for instance, consider it simply as inversion of a very large sparse matrix, albeit a complex and not necessarily square one. A better approach seems to be to consider it a problem in adaptive control, or so-called "machine learning". Such a process, described by Stoll,[24] involves first of all the usual procedure of successive over-relaxation--that is, the mesh is repeatedly

scanned by columns and the value of E at each point modified according to the above equations, without regard to whether some neighboring values have been modified on the current scan or not. If this process converges, it can be carried on until some convergence criterion is satisfied; Stoll suggests the maximum difference in E's at any point between successive scans be less than some selected value. In the present problem, it might be better to have a more stringent condition applying to the region of greatest interest near the origin than elsewhere. The criterion might apply to the real and imaginary parts separately, or might just be made to apply to the modulus. This simple process can be greatly speeded up by increasing the field change after every scan by some (complex) convergence factor of modulus greater than unity. After every few scans, this factor can be modified according to the results so far obtained. Implementing such an adaptive control technique for a complex field is rather tricky, but a surprisingly simple method which has worked successfully on a number of problems has been developed by Stoll. It is attractive to consider also the possibility of gradually varying some of the other parameters in the problem simultaneously. For instance, one might gradually vary the resistivity ratio P from an initial value of one, for which the solutions have been determined in Section 2.3, down to its actual value of .05. We have prepared computer subroutines for evaluating the electric fields at the mesh points in the above equations, for cycling through the relaxation procedure with arbitrary convergence factor, for initialization, and for suitable input and output, but we have not programmed the adaptive control techniques just described.

It might be possible to modify the techniques described in this section to estimate the fields in the RMGS configuration by replacing the meniscus by a right-angled bend.

2.7 Thermal Effects

In this section we shall consider separately heating effects arising from the eddy currents in the silicon and those resulting from the current in the shaping coil.

2.7.1 Eddy Current Heating in Si Ribbon

Eddy currents strong enough to shape a thin ribbon will also be strong enough to heat it significantly. In this section we consider the effect of this heating on the position of the solid-liquid interface and on the maximum steady-state temperature in the ribbon.

The statement made in Section 1.3 that only steady-state temperature conditions need be considered requires some additional support in view of the presence of the liquid-solid interface, which cannot be moved without supplying the latent heat of 1.8 MJ/kg (Table I). From Table III, we see that the power input will be around 2-3 kW. Anticipating some later results of this section, we find the amount of reradiated power is at the most .5 kW, and might be somewhat smaller. The small dimensions of the ribbon, the high temperature of the melt, and the lower thermal conductivity of the solid will limit conduction losses (this again may be justified a posteriori from results below); so most of 1.5 kW net input power should be available to move the interface. The initial velocity of the interface can be determined from

$$P_{net} = L_V A u_I \quad , \tag{2.7.1}$$

where L_V, the latent heat per unit volume, is about 4.5 GJ m^{-3}, and the ribbon cross-sectional area A is taken as 2.4×10^{-5} m^2. Thus $u_I \approx 1.5$ cm/sec. Since this is much larger than anticipated pull rates,[2] we anticipate that the interface, if initially at the shaper plane, would very rapidly move to its steady-state position. It is interesting to note that this position does not depend on the latent heat, which only affects the dynamics of the interface.

Because the ribbon is so thin, the temperature variation across it can easily be neglected. Also since there will be little radiation from the ribbon edges, the temperature will vary but little across the breadth of the ribbon. Thus we have a problem of steady-state heat transfer in one dimension--the pulling direction, with radiation from the ribbon surface and heat produced within it. To avoid analytical complexity we shall assume that the heat is produced uniformly within a region of width H, as we assumed in discussing the degree of shaping. The bulk of the melt, where the temperature will be fixed at T_m, the melting temperature, will be taken as at a distance L from the plane of the shaper. The change in ribbon thickness near this point will be neglected; this can be shown to be insignificant. At large distances along the solid ribbon, the temperature will approach the ambient, which since it will be relatively low we shall take as zero. The overall situation is thus as depicted in Fig. 2.7.1.

The power radiated from a strip of ribbon of height Δx is given by $P_{rad} = 2W \Sigma\varepsilon (T-T_o)^4$, where Σ is the Stefan-Boltzmann constant and T_c the temperature of the surroundings. The heat transfer problem may be simply solved analytically if we can make a linear approximation to the quadratic temperature dependence. When the temperature change from the ambient is small, the approximation

$$(T-T_o)^4 \approx 4T_o^3(T-T_o)$$

is frequently used, but in the present situation, where the temperature change is large and $T_o \approx 0$, this is clearly inadequate. The linear approximation can still be used, though, if we define a fictitious temperature T^* such that

$$T^4 \approx 4T^{*3}T \quad , \tag{2.7.2}$$

where we have set $T_o = 0$, and where T^* is determined self-consistently in such a way that the radiation at temperatures near the actual maximum operating temperature is given accurately. If T^* is chosen such that radiation at the maximum temperature anywhere in the ribbon is given correctly then the overall radiation loss is slightly overestimated. The numerical procedure for obtaining the maximum temperature will be seen to be quite straightforward.

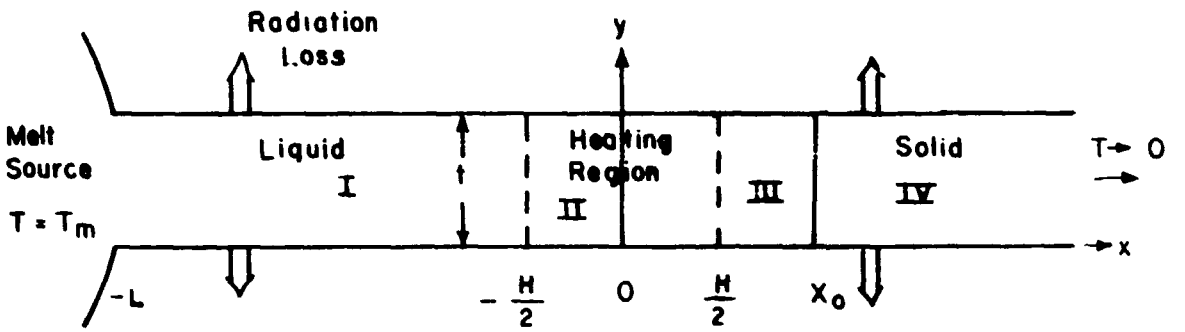

FIG. 2.7.1. GEOMETRY AND TERMINOLOGY FOR STUDY OF HEAT TRANSFER IN RIBBON

Thus in the four regions indicated in Fig. 2.7.1, the heat conduction equations to be solved are simply

$$\frac{\partial^2 T_I}{\partial x^2} = c_1 T_I = 0 \quad , \quad -L < x < -H/2 \quad ; \tag{2.7.3}$$

$$\frac{\partial^2 T_{II}}{\partial x^2} = c_1 T_{II} + c_2 = 0 \quad , \quad -H/2 < x < H/2 \quad ; \tag{2.7.4}$$

$$\frac{\partial^2 T_{III}}{\partial x^2} = c_1 T_{III} = 0 \quad , \quad H/2 < x < X_o \quad ; \tag{2.7.5}$$

$$\frac{\partial^2 T_{IV}}{\partial x^2} = c_s T_{IV} = 0 \quad , \quad X_o < x < \infty \quad , \tag{2.7.6}$$

where

$$c_1 = 2\Sigma \epsilon T^{*3}/tK \quad , \tag{2.7.7}$$

$$c_s = 2\Sigma \epsilon_s T^{*3}/tK_s \quad , \tag{2.7.8}$$

and

$$c_2 = \sigma I^2/(2\pi Hb\delta tK) \quad , \tag{2.7.9a}$$

or if Eq. (2.4.10) holds

$$c_2 = 4\pi^2 \gamma f \beta H^{-1} K^{-1} (\delta/t)^2 \quad . \tag{2.7.9b}$$

For numerical work we will use (2.7.9b) with $t = 4\delta$, $f = 21.1$ MHz, and $H = \pi b/2$. The implicit assumption of these equations that the interface position $X_o > H/2$ will be seen to be well justified.

Eqs. (2.7.3)-(2.7.6) together with the boundary conditions

$$T_I = T_m \quad , \quad X = -L \quad ; \tag{2.7.10}$$

$$T_I = T_{II}, \ \partial T_I/\partial x = \partial T_{II}/\partial x, \ x = -H/2 \quad ; \tag{2.7.11}$$

$$T_{II} = T_{IV}, \ \partial T_{II}/\partial x = \partial T_{III}/\partial x, \ x = H/2 \quad ; \tag{2.7.12}$$

$$T_{III} = T_{IV}, \ K \partial T_{III}/\partial x = K_s \partial T_{IV}/\partial x, \ x = X_o \quad ; \tag{2.7.13}$$

and

$$T_{IV} \to 0, \ x \to \infty \quad , \tag{2.7.14}$$

are readily solved. We shall not present the general solution, but just give the temperature at the solid-liquid interface

$$T_i = T(x = X_o) \doteq \frac{T_m + 2R \sinh Z_H \sinh Z_L}{S \sinh (Z_o + Z_L) + \cosh (Z_o + Z_L)} \qquad (2.7.15)$$

and the maximum temperature in the ribbon

$$T_{max} = T(x = 0) = R(1 - \cosh Z_H) + T_i (S \sinh Z_o + \cosh Z_o) \quad . \qquad (2.7.16)$$

In these equations,

$$R = \pi\gamma f/(4\Sigma \epsilon T^{*3}) \quad , \qquad (2.7.17)$$

$$S = (K_s \epsilon_s / K\epsilon)^{1/2} = 0.63 \quad , \qquad (2.7.18)$$

$$Z_L = c_1^{1/2} L \quad , \qquad (2.7.19)$$

$$Z_H = c_1^{1/2} H/2 \quad , \quad \text{and} \qquad (2.7.20)$$

$$Z_c = c_1^{1/2} X_o \quad . \qquad (2.7.21)$$

If $T^* = 10^3$ K, then with the other assumptions as before, $R = 4.21 \times 10^5$ K and $c_1^{1/2} = 0.92$ cm^{-1}. Because of the asymmetry of the problem, T_{max} might actually be slightly away from $x = 0$, but we can safely ignore this. To solve (2.7.15) and (2.7.16), we assume a value of T_{max}, calculate $T^* = T_{max}/4^{1/3}$, determine R and S, determine Z_o numerically from (2.7.15) assuming there is no supercooling so $T_i = T_m$, and calculate T_{max} from (2.7.16). The true T_{max} will lie between that assumed and that calculated, and can be found with only a few guesses. We carried this procedure out for L = 4 cm and L = 0.4 cm (about the largest and the smallest values one might wish to consider[11]) and for b = 0.5 mm and 2 mm. Even for the smaller value of b, we found $X_o \approx 0.3$ cm for both values of L and T_{max} of 3700-3800 K, well above the silicon boiling point (at 1 atmosphere) of 3060 K. Thus it appears that the interface will generally be well out of the heating region, and also that some auxiliary cooling method will be necessary to keep the silicon at a reasonable temperature. Such cooling would bring the interface closer to, but probably not into, the heating region.

2.7.2 Thermal Balance in Shaper Coil

In this section, we consider the problem of heat production and dissipation in the fine shaping coil, which we will consider to be a simple hairpin. We will show that wires small enough to put close enough to the melt for effective shaping will not be able to lose enough heat by radiation to keep from melting at the current densities required. We will also consider the possibility of cooling the wire by making it a hollow tube with fluid flowing through it, and show that there is some possibility of cooling with flowing gas. We were not able to make a realistic estimate for cooling with a liquid flowing through the tube, but believe it might be feasible. Cooling might also be accomplished by partially embedding the coil in a high-thermal-conductivity, low-electrical-conductivity heat-pipe material; this possibility has not been investigated in any detail.

We will make the following assumptions:

1) We will neglect the large incident thermal flux from the ribbon itself, and only consider the heating by the current in the wire. Although in some circumstances a good part of the incident flux (peaked around 1 to 1.7 μm) might be reflected, in general the only justification for this assumption is that it makes the problem much easier to solve, and in a more complete analysis it ought to be included.

2) The radial dependence of the ac current density can be ignored as far as the thermal, rather than electromagnetic, part of the analysis is considered. This can be shown to be a very small effect.

3) The temperature dependence of the resistivity and thermal conductivity of the shaper wire can be neglected. It can be seen that if these effects are not negligible, they will make the wire more difficult to cool.

4) The wire radius a is much larger than the skin depth in the wire. The bend in the coil can be ignored. These are safe assumptions.

5) The wire is made of copper, of nominal properties as follows:

melting point, $T_m = 1356$ K,

resistivity $\rho_{dc} = 1.7 \times 10^{-8}$ ohm-m,

skin depth $\delta_{Cu} = 14.3$ μm (at 21.1 MHz),

thermal conductivity $K_{Cu} = 3.9 \times 10^{2}$ W m^{-1} K^{-1} .

We will suppress the subscripts ("dc" and "Cu") in the equations. It is doubtful that a better metal than copper can be found for the wire. As frequently mentioned, a practical shaper may also include some sort of graphite or similar concentrator, whose thermal properties should be included in the overall analysis; but it is instructive to see just what is required of the coil itself.

The steady-state temperature in the wire will be given by an equation of the form[25]

$$T = A + B \ln r - \frac{A_0 r^2}{4K} \quad , \tag{2.7.22}$$

where r is the radial distance from the center of the wire and A_0 is the power generated per unit volume. For $a \gg \delta$,

$$A_o = \frac{(I^{rms})^2 \rho}{2\pi^2 a^3 \delta} \quad ; \tag{2.7.23}$$

this equation is valid whether the wire is hollowed into a tube or not. A and B are constants to be determined from the boundary conditions. We will examine in turn the two limiting (and relatively simple) cases of cooling by radiation only and cooling by forced convection in a tube.

I. Solid Wire Cooled by Radiation at Surface. In this case, B must be zero and A is determined from

$$K \left.\frac{dT}{dr}\right|_{r=a} = \epsilon \Sigma (T_{r=a})^4 \quad , \tag{2.7.24}$$

where ϵ is the emissivity of the copper surface, Σ is the Stefan-Boltzmann constant, and we have assumed radiation into a medium at zero temperature. We readily obtain

$$T = \frac{A_0(a^2 - r^2)}{4K} + \left(\frac{A_0 a}{2\epsilon\Sigma}\right)^{1/4} \quad . \tag{2.7.25}$$

The maximum temperature at the center of the wire may be written as

$$T_{max} = T_1 + T_s \quad , \tag{2.7.26a}$$

where

$$T_1 = A_0 a^2/4K \quad , \tag{2.7.26b}$$

and T_s, the surface temperature, $= (A_0 a/2\epsilon\Sigma)^{1/4}$. (2.7.26c)

It is not hard to show that for the situations of interest T_1 will be less than one degree and can safely be neglected. (To be explicit,

$$T_1 = 3.83 \times 10^{-5} (I^{rms})^2/a \quad ,$$

where T_1 is in K, I^{rms} in A, and a in mm). Also we find that for a shiny copper surface ($\epsilon \approx .02$), the wire will immediately fuse at any power levels we have considered; so we will assume the surface is oxidized ($\epsilon \approx .6$) or covered with some highly emitting material ($\epsilon \approx 1$). This of course will make the surface a better absorber of radiation from the molten Si, but as previously stated, we will not attempt to take this into account. By setting $T_s = T_m$, we can calculate roughly the minimum wire radius a_{min} for a given current. The current, in turn, can be related to the wire-to-melt distance b for shaping the ribbon to 400 μm thickness at 21.1 MHz, the conditions principally discussed in earlier sections. The results are shown in Fig. 2.7.2. Of course unless $a < b$, the wire cannot be fitted in next to the melt. It is apparent that even for $\epsilon \approx 1$, the wire must be made quite large and moved rather far away from the melt if it is not to melt itself. The overall power requirements for the various situations were discussed in Sec. 2.5. Since all our assumptions have been such as to neglect effects that would tend to raise the temperature more than we have calculated, it appears that it will not be possible to rely on radiative cooling of the shaper wire.

II. Hollow Tube with Internal Fluid Cooling. We assume the shaper is a cylindrical tube of interior radius a_1 and exterior radius a. We will now assume there is negligible radiation at the outer surface ($\epsilon \approx 0$), to simplify the discussion. At the inner surface, we will take as the boundary condition

$$\left.\frac{dT}{dr}\right|_{r = a_1} = \frac{h}{K} \left(T_{r = a_1} - T_f\right) \quad , \tag{2.7.27a}$$

where the heat transfer coefficient

$$h = K_f Nu/2a_1 \quad , \tag{2.7.27b}$$

K_f being the thermal conductivity of the cooling fluid and Nu being the Nusselt number, a dimensionless parameter which we discuss below. T_f can

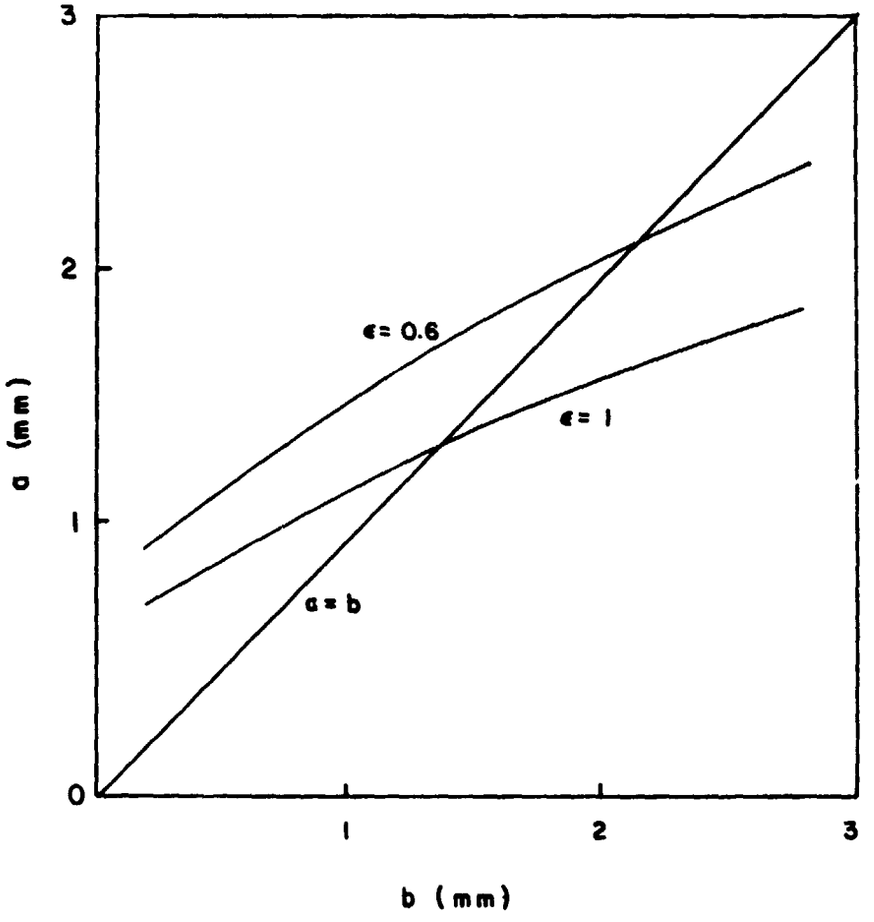

FIG. 2.7.2. RADIATIVE COOLING OF SHAPING COIL. MINIMUM COIL RADIUS TO AVOID FUSION, a, PLOTTED AGAINST COIL-CENTER-TO-MELT-SURFACE DISTANCE, b, FOR SHAPING RIBBON 0.4 mm THICK AT 21.1 MHz. ϵ = EMISSIVITY OF COIL SURFACE.

be taken as the average temperature of the cooling fluid, provided the outlet absolute temperature is not more than 3 times that at the inlet[26]. Evaluating A and B from the boundary conditions, we find

$$T - T_f = \frac{A_0 a^2}{2K}\left[\frac{2K}{K_f Nu}\left(1 - \frac{a_1^2}{a^2}\right) + \ln\frac{r}{a_1} - \frac{r^2 - a_1^2}{2a^2}\right] \quad . \tag{2.7.28}$$

From this equation, we can show that the temperature difference across the wall,

$T(r=a) - T(r=a_1) < T_1$, where T_1, defined by (2.7.26b), is less than one degree. Thus we consider only the temperature at the inner wall, and write

$$T(r=a_1) - T_f \equiv \Delta T = T_1 \frac{2K}{K_f Nu}\left[1 - \left(\frac{a_1}{a}\right)^2\right] \quad . \tag{2.7.29}$$

If the temperature variation of the viscosity is not too strong, the Nusselt number for most gasses is well approximated by[26,27]

$$Nu = .013\ Re^{0.83} \quad , \tag{2.7.30}$$

in the turbulent flow regime (Reynolds numbers $Re > 3 \times 10^3$). The Reynolds number is given by

$$Re = 2\ a_1 v/\upsilon \quad , \tag{2.7.31}$$

where v is the average flow rate of the gas and υ is its viscosity at the average temperature. Defining the ratio $\lambda = a_1/a$, we see we can write

$$\frac{\Delta T}{T_1} = \frac{2^{.17}}{.013}\frac{K}{K_f}\left(\frac{\upsilon}{av}\right)^{.83}\frac{1-\lambda^2}{\lambda^{.83}} \quad . \tag{2.7.32}$$

λ must be chosen to make the shaper sufficiently strong; let us assume $a = 1$ mm and $\lambda = .5$. Also let us assume that the gas is air, precooled so that the average temperature is room temperature (294K). Then $K/K_f \approx 1.6 \times 10^4$ and $\upsilon \approx .16$ cm^2/sec; so

$$\frac{\Delta T}{T_1} \approx \frac{5.84 \times 10^4}{v^{.83}}$$

where v is given in m/sec. For turbulent flow, v will have to be at least about 50 m/sec. At that rate, $\Delta T/T_1 = 2.3 \times 10^3$. For $a = 1$ mm and $b = 1.4$ mm,

$T_1 \approx .46$ K, hence the wall temperature would rise to 1336 K, or just a bit below the melting point. Since this might be brought down by higher flow rates and by conduction and radiation losses, it seems as if cooling with a gas might be possible for a shaping wire of the dimensions assumed. It is not likely that smaller wires closer to the melt could be cooled this way though, despite their carrying smaller currents. We attempted to make a similar analysis for cooling by a liquid, but found ourselves in an inconsistent range of parameters for use of the appropriate generalization of (2.7.30). One would expect, though, that if cooling with a gas is feasible, cooling with a liquid at lower flow rates would also work.

2.8 Summary and Conclusion

We have described methods of calculating fields and forces induced in a silicon ribbon by a simple hairpin-shaped coil. We have determined the current and power necessary to produce ribbon of a specified thickness by electromagnetic shaping, both for an isolated ribbon and for a ribbon being drawn from a nearby levitated spherical melt In both cases the current required for shaping to .4 mm thickness is larger than has been previously thought--in the range of 100 A. For the isolated ribbon, the power required is also large, but for the ribbon drawn from the levitated sphere, the total power is only a few kilowatts. Departure of the melt from a flat ribbon shape, location of the freezing interface far from the shaping plane, and excessive heating of the ribbon by the eddy currents may all be severe problems which will have to be overcome in any practical system. Numerous simplifications and approximations have been made in the course of these calculations, but it is extremely doubtful that more accurate calculations would alter qualitatively any of the conclusions presented here.

3. OTHER INNOVATIVE PROCEDURES

3.1 Introduction

The object of this task has been the evaluation of possible means for shaping silicon ribbon other than using electromagnetic forces, and making a detailed analysis of those methods which appear most feasible from the standpoint of space production. Emphasis was placed more on developing understanding of the physical mechanisms of importance and on establishing high-feasibility concepts for shaping than on engineering design.

By way of introduction, we shall describe three techniques used for shaping materials (terrestrially) from the melt: the web-dendrite, the EFG (Edge-Defined Film-Fed Growth), and the Pilkington Float Glass methods.

Web Dendrites

In this process, a seed crystal is induced to form two dendrite arms, which are curved down into the melt by surface forces imposed by the liquid material. Soon after the start of growth, the two dendrites form what is essentially a parallel frame, supporting a web of liquid which freezes shortly above the surface of the liquid. The web material has a twinned structure, and the crystallographic orientation in the plane of the sheet is off a close-packed orientation as a consequence of the dendritic growth process. Growth rates are of the order of 5 cm/sec. One of the problems associated with this method is that, as a result of liquid drainage induced by gravity, the material does not have a uniform thickness. Hence, the cooling rate is not uniform, and thermal stresses are induced unless cooling rates are extremely well controlled. Generally, at web widths of about 3 cm the dislocation structure induced by thermal stresses is so great that the web becomes polycrystalline. Furthermore, the dendritic growth process results in variations in the concentration of alloying elements across the width of the web. In addition, because dendritic growth is unconstrained, the process is rather delicate to control.

EFG

Liquid material is drawn into a die by capillarity forces. From the pool in the top of the die, it is drawn out by a seed crystal in a manner analogous to the Czochralski method. The liquid departs from the die with a shape defined by bounding vertical (in the direction of pulling) surfaces.

In principle, if this method were developed properly, the material would have properties closely comparable with the best Czochralski material. In this case, it would suffer from two main drawbacks. First, the amount of yield would be limited by stability considerations. This drawback is overcome, to some degree, by using multiple growth slots. Second, the dies wear excessively, and the die cost forms a significant amount of the material cost. We see another possible disadvantage for future development, i.e., there is a lower limit to the ribbon thickness produced by this method, which we estimate to be about 120 μm.

Pilkington Float Glass Process

Molten glass flows out of the melting tank, over the surface of a tank of molten tin. As it flows over the tin its temperature gradually falls until it becomes solid. It then passes over a weir, onto a conveyer, where it is cut into convenient lengths.

3.2 Factors Affecting Ribbon Formation

Let us now consider the relative importance of the various factors which affect ribbon formation in space. In particular, we include (1) capillarity effects, which tend to alter the shape of the liquid until minimization of net interfacial energy of the entire system is achieved, (2) viscous effects which tend to retard the flow of the liquid, (3) flow forces resulting from the fact that the liquid is in motion, and (4) accelerational effects within the liquid. We shall demonstrate that, for liquid silicon, the first of these factors is dominant over the last three.

3.2.1 Capillarity Forces Versus Viscous Forces

Let us first compare the relative influence of capillarity forces in a liquid-silicon system, as opposed by viscous forces. We shall consider a relatively simple example for which a quantitative treatment is available, i.e., the spreading of a viscous liquid drop on a planar solid surface under the action of interfacial forces. We use here the results of the theory of "wetting" kinetics developed by Strella[28] and extended by Markworth and Glasser[29]. They considered the problem of a liquid drop, initially spherical and touching the planar surface at only one point, as it subsequetly spreads over the surface, finally attaining its equilibrium configuration. In particular, they showed that

$$\frac{\alpha\, t}{4^{1/3}\,\eta\, R_o} = f(\theta,\theta_\infty) \quad , \tag{3.2.1}$$

where α is the surface tension of the drop, η its viscosity, R_o its initial radius, t is the time measured relative to the initial condition, for which $t = 0$. θ is the instantaneous contact angle between the drop and the surface and is measured relative to the planar surface not in contact with the drop, and θ_∞ is the equilibrium contact angle. (The contact angle θ approaches θ_∞ in the limit as t approaches infinity[28,29]. It can be seen, from Eq. (3.2.1), that, as expected, high values of α lead to correspondingly high rates of approach to equilibrium, whereas high η leads to slow rates. The functional form of $f(\theta,\theta_\infty)$ is unimportant for the present work[29] but one could show, with the help of results reported in Refs.(28) and (29), that the spreading process is generally largely complete at times such that this function has a value of roughly 5. Hence, defining τ as the time required for the function to attain this value, we find,

$$\tau = 5 \cdot 4^{1/3}\, \eta\, R_o/\alpha \quad .$$

Using the values $R_o \approx 1$ cm, $\eta \approx 0.02$ poise, and $\alpha \approx 720$ dyne/cm, we find that τ is of the order of 10^{-4} second, so that surface forces in liquid silicon generally overcome retarding viscous forces extremely quickly. That this is so is, however, not surprising in view of the relatively high surface tension of liquid silicon and its relatively low viscosity--for example, the viscosity of water is only about a factor of two smaller than the value used here for liquid silicon.

3.2.2 Capillarity Forces Versus Accelerational and Flow Forces

We shall use a somewhat different approach to evaluate the comparative effects of capillarity forces versus accelerational and flow forces. In particular, we consider two of the various dimensionless parameters that are commonly used to identify behavior similarities among systems of different size and also to define different regimes of behavior; these two parameters are the Bond number, Bo, and the Weber number, We, defined as

$$Bo \equiv \rho a L^2/\gamma$$

$$We \equiv \rho L V^2/\gamma$$

where ρ is the fluid density, a its acceleration, V its velocity, L a characteristic length, and γ the fluid surface tension. The Bond number defines regimes in which either acceleration or capillarity forces dominate, whereas the Weber number compares flow forces and capillarity forces. The appropriate hydrodynamic regimes can be illustrated graphically (see Reynolds[30] and Otto[31]) on a plot of Bo versus We, as shown in Fig. 3.2.1. Assuming, for liquid silicon, order-of-magnitude-estimated values for ρ, a, L, V, and γ of 1 gm/cm^3, 1 cm/sec^2 ($\sim 10^{-3}$ g), 1 cm, 10^{-2} cm/sec (roughly the anticipated pull rate), and 10^3 dyne/cm, respectively, we find We $\sim 10^{-7}$ and Bo $\sim 10^{-3}$. The point in Fig. 3.2.1 characterized by these numbers can be seen to lie deeply within the "capillary-dominated" region, indicating again that capillarity forces in low gravity play a dominant role in controlling the instantaneous shape of the liquid-silicon system.

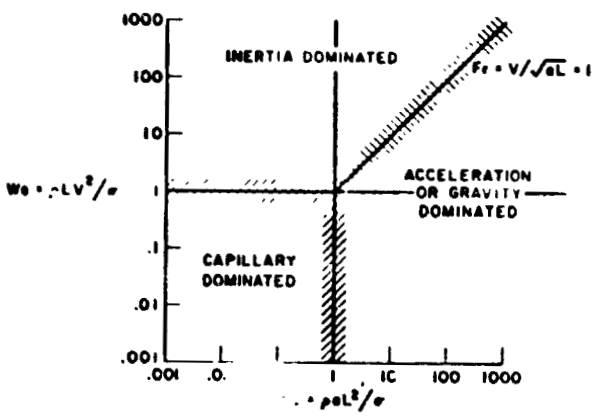

FIG. 3.2.1. HYDRODYNAMIC REGIMES (AFTER REYNOLDS AND OTTO). THE QUANTITY Fr IS THE FROUDE NUMBER, WHICH IS EQUAL TO $(We/Bo)^{1/2}$.

3.3 Use of Capillarity Forces to Shape Silicon Ribbon

3.3.1 Capillarity-Induced Interaction Between Solids and Liquids

From a very general point of view, the shaping of liquid silicon into ribbon via capillarity forces, would be achieved through the interaction of the liquid with an appropriate arrangement of solid surfaces. Assuming that interfacial forces control the shape of the liquid, the shape would be that for which the net interfacial energy of the system (liquid plus solids with which the liquid comes into contact) is minimized. Unfortunately, the problems that one encounters in determining the minimum-energy configuration for a relatively complex system are generally exceedingly difficult. Indeed, it has been pointed out by Nitsche[32] that only in 1951 was it proven that a sphere-like surface (certainly a simple system from the point of view of the more complex arrangements needed for ribbon shaping) having constant mean curvature must in fact be a sphere. To illustrate the approach that one can take in calculating capillarity-driven equilibrium solid-liquid configurations, we shall consider here the simple, but important and pertinent, problem of calculating the equilibrium configuration of a quantity of liquid situated on a rigid, spherical solid surface.

The system we are considering is illustrated schematically in Fig. 3.3.1. The droplet shape, along the liquid-vapor surface, is characterized by constant curvature, and the locus of points describing the boundary between the solid-vapor surface and the solid-liquid interface is a circle. All angles and radii of curvature are taken as positive for the specific configuration illustrated in Fig. 3.3.1, and their signs would be altered in appropriate fashion for concave interfaces. Let us suppose that the radius of the liquid system in a free, and therefore spherical, configuration is r. Then, it is relatively easy to show that the change of interfacial energy, ΔE_i, brought about by "attachment" of the liquid to the surface, is given by

$$\Delta E_i = 2\pi\rho^2 \gamma_{\ell v} [1 - \cos(\theta + \alpha)]$$

$$+ 2\pi R^2 (\gamma_{\ell s} - \gamma_{sv}) (1 - \cos\alpha) - 4\pi r^2 \gamma_{\ell v} \qquad (3.3.1)$$

where ρ is the radius of curvature of the liquid-vapor interface after attachment to the solid has occurred, R is the radius of curvature of the solid, and $\gamma_{\ell v}$, γ_{sv}, and $\gamma_{\ell s}$ are the respective free energies per unit area associated with the liquid-vapor, the solid-vapor, and the solid-liquid interfaces. The angles θ and α are defined in Fig. 3.3.1, from which we note that θ is the "contact angle" between the liquid and the solid. The angles are all taken as positive for the configuration illustrated in the figure.

Now the <u>equilibrium</u> configuration of the system is that for which ΔE_i is minimum (we are assuming zero gravity) subject to the constraint that the volume of the liquid remains constant upon attachment to the surface. To evaluate the nature of this configuration, we employ Lagrange's method of undetermined multipliers and define a quantity Ψ such that

$$\Psi \equiv \Delta E_i + \lambda (V_a - V_f) \qquad (3.3.2)$$

where λ is a Lagrange multiplier, V_a is the volume of the attached liquid, and V_f is the volume of the free liquid. Now, one can readily show that

$$V_a = \frac{4\pi\rho^3}{3} \xi(\theta + \alpha) - \frac{4\pi R^3}{3} \xi(\alpha) \quad ; \qquad (3.3.3)$$

$$V_f = \frac{4\pi r^3}{3} \quad ; \qquad (3.3.4)$$

where

$$\xi(x) \equiv 1/2 \left(1 - \frac{3}{2}\cos x + 1/2 \cos^3 x\right).$$

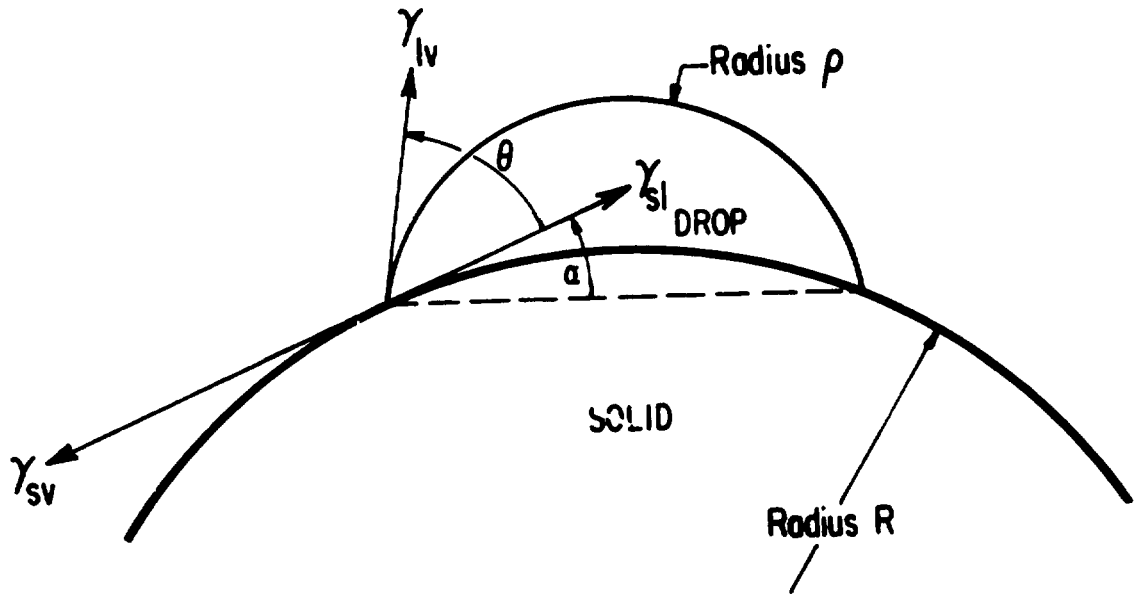

FIG. 3.3.1. ILLUSTRATION OF THE INTERACTION OF A QUANTITY OF LIQUID WITH A SPHERICAL SOLID SURFACE

In addition, we see from Fig. 3.3.1 that

$$R \sin \alpha = \rho \sin (\theta + \alpha) \quad . \tag{3.3.5}$$

Combining Eqs.(3.3.3) and (3.3.5),

$$V_a = \frac{4\pi R^3}{3} \left\{ \frac{\sin^3 \alpha}{\sin^3(\theta+\alpha)} \xi(\theta + \alpha) - \xi(\alpha) \right\} \tag{3.3.6}$$

Next, combining Eqs.(3.3.1) and (3.3.5),

$$\Delta E_i = 2\pi R^2 \left\{ \frac{\gamma_{\ell v} \sin^2 \alpha}{\sin^2(\theta+\alpha)} [1 - \cos(\theta + \alpha)] + (\gamma_{\ell v} - \gamma_{sv})(1 - \cos \alpha) \right\} - 4\pi r^2 \gamma_{\ell v} \quad . \tag{3.3.7}$$

Eqs. (3.3.2), (3.3.4), (3.3.6), and (3.3.7) can be combined to yield an expression for Ψ entirely in terms of the variables α and θ (treating r, R, and the interfacial energies as fixed parameters).

The minimum value of ΔE_i is determined by setting

$$d\Psi = \frac{\partial \Psi}{\partial \theta} d\theta + \frac{\partial \Psi}{\partial \alpha} d\alpha = 0 \quad , \tag{3.3.8}$$

and hence by equating each of the partial derivatives in (3.3.8) to zero. First, setting $\partial\Psi/\partial\theta = 0$ and solving for λ, we obtain

$$\lambda = \frac{-2\gamma}{R} \frac{\sin(\theta + \alpha)}{\sin \alpha} \quad . \tag{3.3.9}$$

It is interesting here to observe that Eqs. (3.3.5) and (3.3.9) can be combined to yield

$$\lambda = -2\gamma/\rho$$

so that λ is simply the negative of the "Laplace pressure" associated with the attached liquid. Next, we set $\partial\Psi/\partial\alpha = 0$ and subsequently eliminate λ in the resulting expression by means of (3.3.9). We thus obtain

$$\gamma_{sv} = \gamma_{\ell s} + \gamma_{\ell v} \cos \theta \quad . \tag{3.3.10}$$

Eq. (3.3.10) which is identical to the familiar equation of Young and Dupre′, describes the relation between the equilibrium contact angle and the various interfacial energies. This expression has been derived here for the special case in which the solid surface is spherical, although the same form for this relationship has been obtained for other situations as well (e.g., liquids contained within closed axisymmetric containers[33]). It will prove to be essential for use in evaluating the equilibrium configuration associated with the more complex systems which would be used to shape liquid silicon into ribbon.

We note, in concluding this analysis, that Darbro[34,35] has discussed a number of important concepts relative to phenomena associated with the nature (particularly under low gravity conditions) of such things as liquids, liquid films, liquid-solid interactions, and the solidification of liquids.

3.3.2 Melt Containment

For the shaping of ribbon from a bulk melt, it will be important to control the shape of the liquid-vapor interface at the melt surface. Because of the dominance of capillarity forces, the shape of the interface is controlled by the shape of the container as well as the contact angle θ. To illustrate the manner in which shape control can be achieved, we consider the problem of obtaining a flat liquid-vapor interface, although the procedures we describe apply equally well to obtaining interfaces having non-zero curvature. We shall assume that the Young-Dupre′ equation, as derived above for the interaction of a liquid with a spherical (concave or convex) solid surface, applies to other curved surfaces as well[33].

One possible configuration, for which the container is spherical, is illustrated in Fig. 3.3.2. The principal drawback here is that a flat liquid-vapor interface can be obtained for only one depth of liquid, as illustrated in the figure. If the container holds either more or less than this particular amount of liquid, then the liquid-vapor interface will be

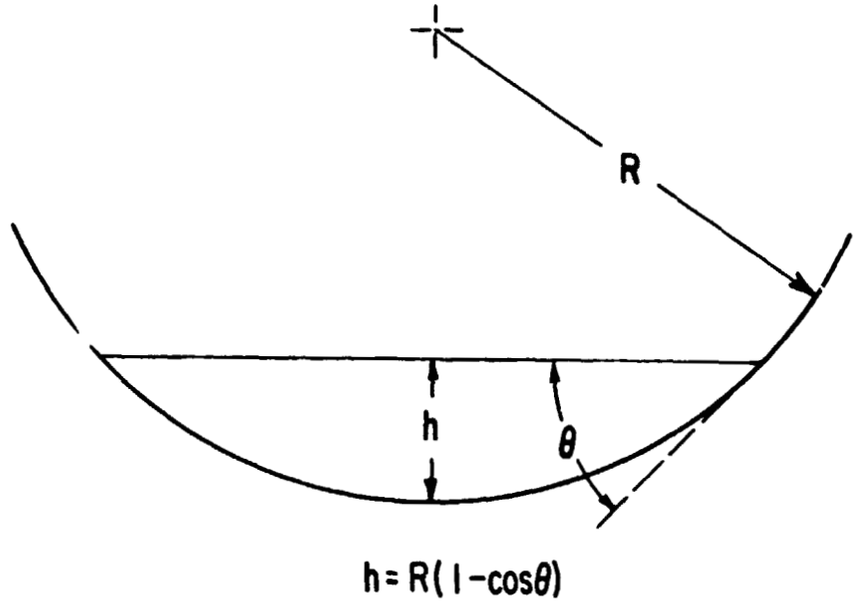

FIG. 3.3.2. RELATION BETWEEN DEPTH L AND CONTACT ANGLE θ IN ORDER TO ACHIEVE A FLAT LIQUID-VAPOR INTERFACE INSIDE A SPHERICAL CONTAINER OF RADIUS R.

curved (concave upward for the former case, convex upward for the latter). A more practical arrangement is shown in Fig. 3.3.3. Here the container is a surface of revolution, the walls forming a circular cone over at least some region, the apex angle ϕ of the cone, as illustrated in the figure, being $\pi - 2\theta$. For this situation, the liquid-vapor interface will be flat for any liquid depth as long as the interface intersects the container within the region that is circularly conical.

The above examples illustrate the importance of container shape in obtaining liquid-vapor interfaces having given desired curvature. It is clear, however, that the problem is one which can be met by suitable choice of container material and shape.

3.3.3 Capillarity-Driven Ribbon Formation

We shall now describe a general concept for ribbon formation based on the assumption that interfacial-energy effects control the shaping process. In particular, we shall utilize a crystallization process which is "constrained"*, so that the material produced can, in principle, be of the highest quality. The two key features of the process are the following:

1. A framework is used to draw liquid sheet from a bath in a manner analogous to the role played by the dendrites in the web process.
2. Constrained growth is coupled with rapid rate of production by pulling the crystal in a direction aligned at an angle to the growth direction.

(We note that the benefits offered by the low gravity environment of an orbiting spacecraft relative to constrained crystal growth have been discussed elsewhere[36] for the particular case of the growth of beta alumina from the melt under low-g conditions.)

---

* Constrained crystal growth is that for which the molten material ahead of the solid-melt interface is [illegible]e, i.e., above the melting point, as opposed to the case of unconstrained crystal growth for which the liquid ahead of the growing crystal is metastable, i.e., below its equilibrium freezing temperature. Freezing occurs in the constrained-growth situation as a result of the isotherm corresponding to the freezing temperature being moved relative to the melt. Maintenance of constrained growth prevents the solid-melt interface from breaking down. If, however, the growth rate becomes too fast, the interface becomes cellular; and in the limit of even faster growth rates, it becomes dendritic. If, however, the growth rate becomes too fast, the interface becomes cellular; and in the limit of even faster growth rates, it becomes dendritic.

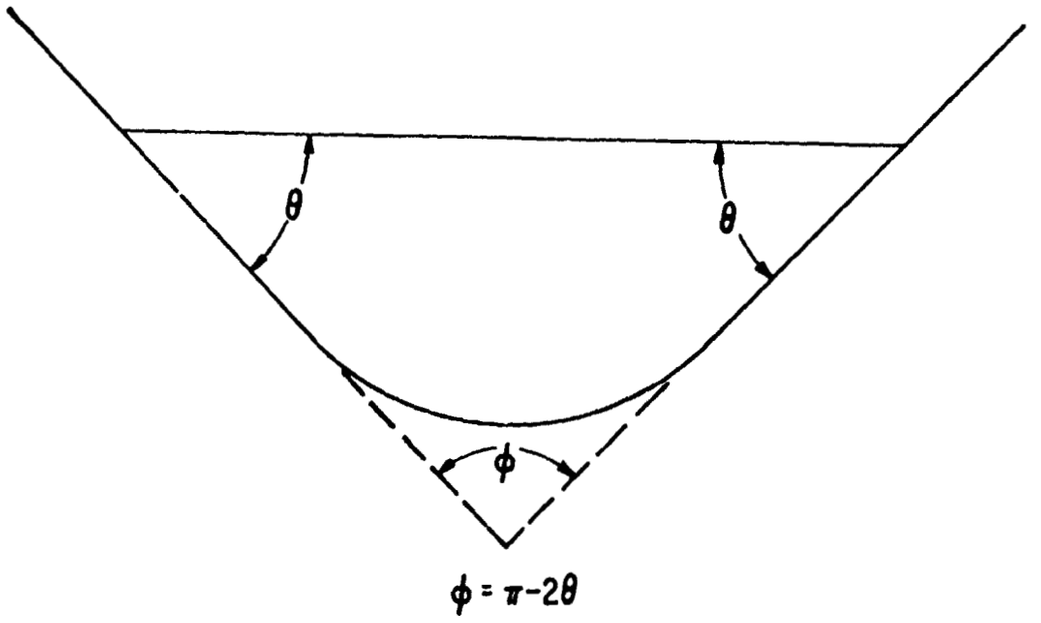

FIG. 3.3.3. RELATION BETWEEN APEX ANGLE ϕ AND CONTACT ANGLE θ IN ORDER TO ACHIEVE A FLAT LIQUID-VAPOR INTERFACE INSIDE A CONTAINER WHICH IS A RIGHT CIRCULAR CONE OVER A PORTION OF ITS SURFACE.

Aspects of this process are discussed below in more detail together with our view of some of the attendant problems. The concept of "off-angle" growth, mentioned under (2), above, is sufficiently important in its own right to be described in a separate section, which follows below.

The basic procedure for utilizing capillarity forces to produce ribbon is illustrated schematically in Fig. 3.3.4. The melt is drawn up in the desired ribbon shape, along a frame which defines its boundaries. The frame could, in principle, either be stationary or move with the liquid at a rate such that the liquid ribbon does not move relative to the frame. A stationary frame would result in a simpler experimental apparatus, but a movable frame would undergo less wear due to frictional effects resulting from the surrounding moving liquid; in addition, deleterious boundary-layer effects in the moving liquid would be minimized if the frame is also moving. Solidification of the liquid could be induced either before or after the ribbon is separated from the frame. Some particular aspects of this concept that would require further consideration are described below:

Film Stability. Viscous forces, as we have shown, tend to be small compared to capillarity forces; but they do exist and do tend to oppose film formation, and the extent to which these forces constitute a threat to film stability constitutes a problem which must be analyzed. For the web dendrite process, which in this respect is a close analog of the proposed process, pull rates of about 5 cm/sec have been attained despite the supercooled (and thus more viscous) melt. We anticipate, for the space process, that pull rates of the order of .01 to .02 cm/sec will be attained.

A second stability question is involved with the stability of a thin film or sheet. Without externally applied forces, the liquid film supported by a framework should be stable. If subjected to external vibrations, it could support limited amounts of longitudinal and/or transverse standing-wave systems; these waves would be damped, of course, by viscous flow of material. We did not consider this problem, but the limits of applied vibrations, beyond which the liquid sheet becomes unstable, must eventually be determined as a function of sheet dimensions. The success of the web dendrite method gives us some confidence that the potential stability problems associated with our process can be satisfactorily resolved.

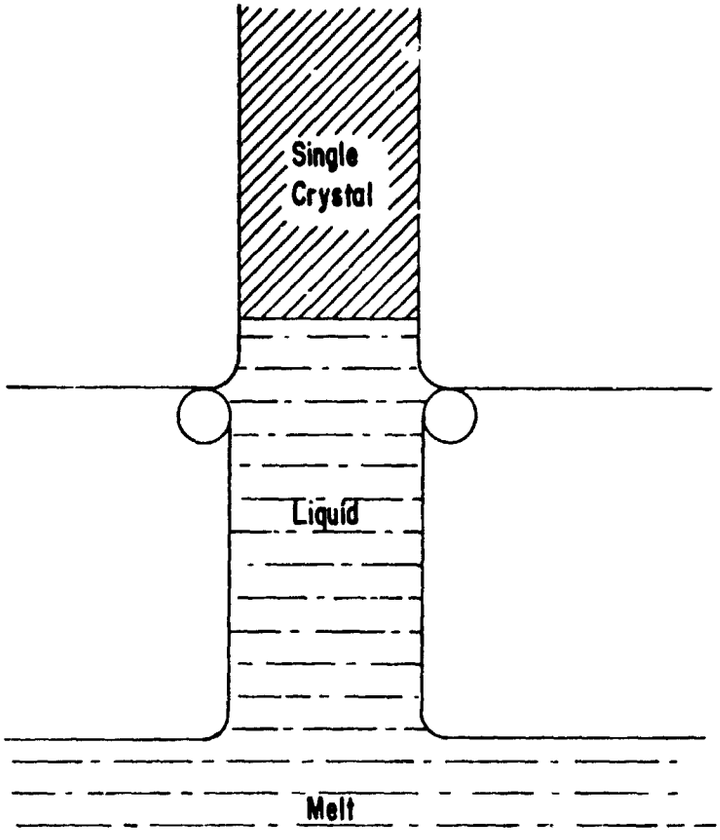

FIG. 3.3.4. SCHEMATIC ILLUSTRATION OF METHOD FOR UTILIZING CAPILLARITY FORCES TO SHAPE LIQUID SILICON INTO RIBBON. THE PLANE OF THE RIBBON, IN THIS DRAWING, LIES IN THE PLANE OF THE PAPER.

Materials for Frame and Crucible. Materials developed for the EFG process should be directly applicable to our work. The most successful has been graphite, which seems to be an obvious first-choice material. Other materials which have been successful are silica and silicon carbide. These materials may need surface treatment in order that they may be "wetted" by the liquid silicon.

Mechanical Stresses. The greatest concern regarding the concept we have developed is related to the mismatch in thermal-expansion properties between the frame and the single crystal formed within it. Our concerns on this ground have been reinforced by the experience of the web-dendrite crystal growers. Our response to this problem is twofold: First, an examination is called for of the difference in the stress distribution between a very thin, wide, film and the less flexible thick, narrow web crystal. Second, some potential practical solutions to this problem exist. These solutions include cutting away the frame closely above the solid-liquid interface region by some mechanical procedure, and the alternative in which the frame is drawn away just before the freezing interface region. The latter method would provide a less flat sheet than one formed between a frame, but would completely remove the thermal-stress problem.

Provided that the frame-stress problems can be satisfactorily removed, other potential sources of stress seem to be less important. For example, since the web crystal growers coiled their crystals continuously on a 90 cm reel, the crystals formed in the space process, which should be thinner, may be coiled at least as tightly.

3.4 Off-Angle Growth

The concept of off-angle growth, mentioned briefly above, offers some important advantages for the production of single-crystal ribbon in space. Suppose a single-crystal ribbon is being grown such that the pull velocity and growth velocity are aligned in different directions. Let V_p be the pull velocity, V_g the growth velocity, and θ the angle between the pull and growth directions. (The quantity θ defined here is distinct from the "contact angle" discussed above, which was also denoted by θ). This concept is illustrated schematically in Fig. 3.4.1. For the configuration shown here, as well as for those illustrated in Figs. 3.4.2 and 3.4.4, it is assumed that the pull direction lies in the plane of the molten sheet; this need not be the case, however, as we shall discuss below (and as is shown in Fig. 3.4.3).

We can use Fig. 3.4.2 to help derive the relationship between V_p, V_g, and θ. Let us define A_g as the actual area of the solid-melt interface (i.e., that normal to the growth direction) and A_p as the interface area projected normal to V_p. In order that mass be conserved, we require that

$$V_g A_g = V_p A_p \quad .$$

But, one can readily see that

$$A_p = A_g \cos \theta$$

so that

$$V_g = V_p \cos \theta \quad .$$

Hence, non-zero value of θ would result in an enhancement of pull rate, i.e., $V_p > V_g$.

Two possible approaches to achieving off-angle growth are shown in Fig. 3.4.3. In one of these, the growth velocity vector is aligned at an angle to the plane of the molten ribbon; in the other, it lies within this plane. (Fig. 3.4.1 and 3.4.2 correspond to the former case.) The latter situation is probably simpler to achieve experimentally, since heat flow within the molten ribbon would occur along the plane of the ribbon.

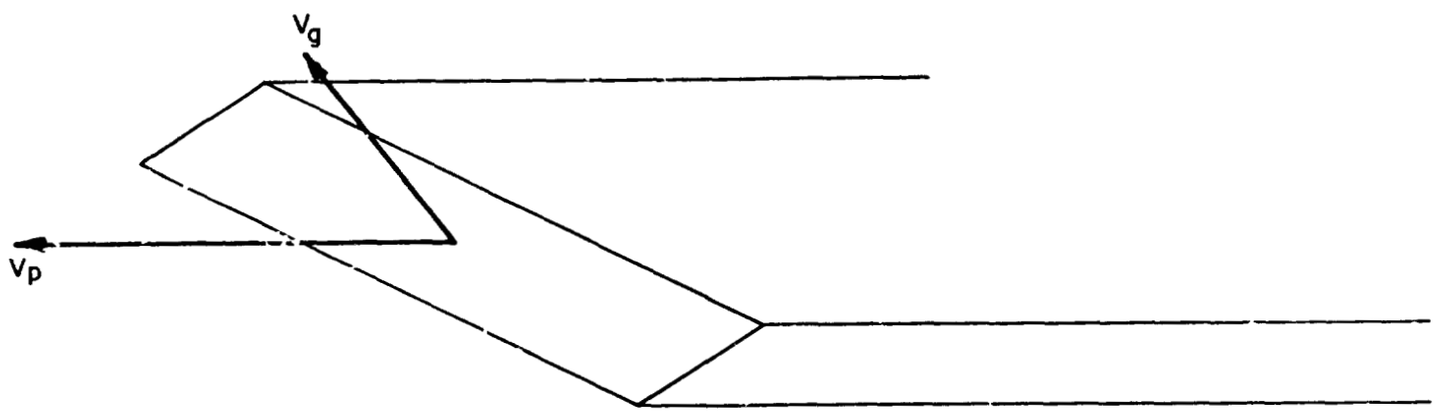

FIG. 3.4.1. ILLUSTRATION OF NONCOLLINEARITY OF PULL DIRECTION AND GROWTH DIRECTION CHARACTERIZING OFF-ANGLE GROWTH. THE MOLTEN RIBBON IS SHOWN TOGETHER WITH THE SOLID-MELT INTERFACE.

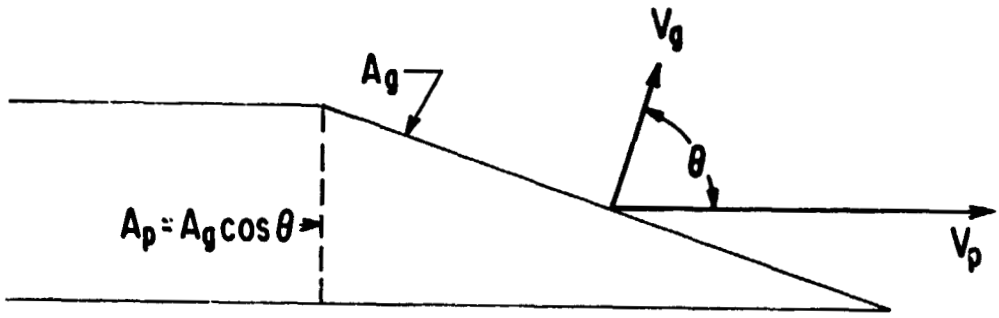

FIG. 3.4.2. ILLUSTRATION OF QUANTITIES USED TO DETERMINE RELATIONSHIP BETWEEN V_g, V_p, AND θ. AN EDGE VIEW OF THE MOLTEN RIBBON IS SHOWN TOGETHER WITH THE SOLID-MELT INTERFACE.

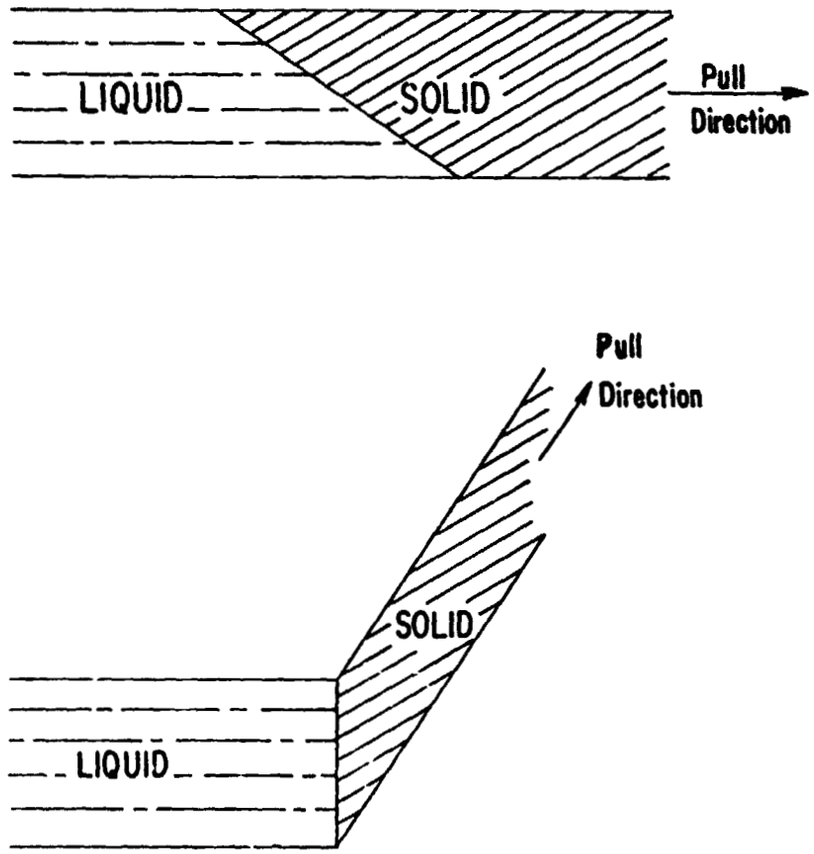

FIG. 3.4.3. ALTERNATIVE CONCEPTS FOR OFF-ANGLE GROWTH

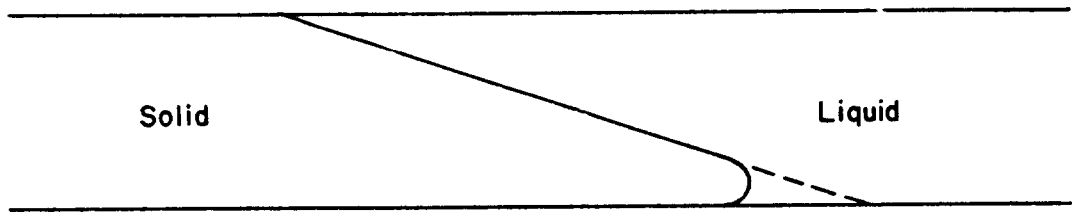

FIG. 3.4.4. EXAGGERATED VIEW OF THE ROUNDING OF THE SOLIDIFIED RIBBON AT ITS MOST POINTED REGION. THIS BEHAVIOR WOULD ALSO CHARACTERIZE THE OTHER OFF-ANGLE GROWTH CONFIGURATION, ILLUSTRATED IN FIG. 3.4.3.

Other problems would exist, however, such as those resulting from the manner in which heat is radiated from various portions of the system; these would have to be treated in subsequent studies.

Advantages to be gained from utilizing off-angle growth for ribbon production include the following:

(1) Enhancement of pull rate.

(2) More homogeneous crystal. Defects (e.g., spiral dislocations) tend to propagate along the growth direction and hence would terminate at the ribbon surface for off-angle growth.

(3) Thinner ribbon. For the case illustrated in Fig. 3.4.2, for which the solidified ribbon and molten ribbon are not coplanar, the solidified material is thinner than the molten ribbon.

(4) Well suited to space processing. The off-angle growth process would be difficult to maintain stably on earth.

The portion of the solidified ribbon which, at the melt-solid interface, is most pointed, has some of the properties of a growing dendrite, and existing dendritic-growth theory is applicable. A sharply pointed surface would be unstable, because of the Gibbs-Thomson effect, and it would tend to become rounded as illustrated in an exaggerated manner in Fig. 3.4.4. The degree of rounding depends, in some measure, upon such factors as the rate of advance of the crystal and upon the crystal-melt interfacial energy. We expect the radius of curvature to lie in the range 1 to 5 μm. One would normally expect an interface of this nature to become irregular; however, thermal constraints would prevent this from happening in the present situation.

It should also be noted that our concept of off-angle growth would lead to a surface exposed along the plane of the sheet which may not be a close-packed orientation. Such an orientation is obtained from web material.

Off-angle growth is thus a potentially useful means for enhancing the rate of ribbon production in space as well as the homogeneity of the material. It should be emphasized, however, that this process is not

essential to the concept described above involving the use of capillarity forces for ribbon shaping. It would be used only if found to be feasible within available technology.

3.5 Conclusion

The processes described above, i.e., the use of capillarity forces to shape silicon ribbon and the application of off-angle growth to produce ribbon at faster rates and greater degree of homogeneity, appear to be feasible from a conceptual point of view. Engineering design problems do exist, such as maintenance of a stable configuration during off-angle growth, and these must be considered as part of further developments. Certainly, the low-gravity environment would have considerable influence upon design considerations.

Additional shaping concepts that also appear to be feasible need to be evaluated against the processes proposed herein. (Indeed, we have considered a number of possible concepts, subsequently discarding them in favor of those described above.) For example, one potential process would involve zone melting, utilizing a spatially fixed molten zone. Polycrystalline sheet would be fed along a given direction, melted within the zone, and single crystal ribbon pulled out from the molten zone. This concept could lead to problems, however, in obtaining a flat solidified sheet. It should be noted that off-angle growth could be utilized with this type of procedure.

4. CONCLUSIONS AND RECOMMENDATIONS

As part of our overall assessment of the prospects for space production of silicon single crystal ribbon, we reviewed the recent literature relating to potential large-scale use of silicon for solar cells and had discussions with a number of researchers active in this field. The results of this survey have been considered in arriving at the following conclusions:

1. There is no doubt that the need exists for much better methods of producing silicon ribbon for solar cells, if photovoltaic conversion is ever to emerge as a viable means of producing large amounts of electricity. Not only are much lower costs required, at almost every stage of the process, but also minimally low energy expenditures, in comparison to the total energy produced by the material over its useful life.
2. There exist a number of competing technologies for production of Si ribbon. Some of these were described in Section 3.1, and others are under development. No process or concept at present has demonstrated any clear superiority, though.
3. No material other than silicon is given serious consideration for large-scale terrestrial solar power conversion, because of i) availability of raw material, ii) good conversion efficiency, and iii) overall knowledge of and experience with the material.
4. As far as production of silicon wafers for integrated circuits goes, it appears that any new process will have to be justified strictly on economic grounds, and moreover will have to dislodge an entrenched, if rather awkward, technology.
5. Current requirements for electromagnetic shaping of silicon ribbon are substantial even if small shaping coils very close to the melt are used Currents in the 100 A range will be required for shaping to 0.4 mm thickness
6. Power requirements for drawing an electromagnetically shaped ribbon from a levitated spherical melt are moderate--a few kW, including losses in both the shaping coil and in the molten silicon, if the shaping coil is small.

7. Power requirements for thinning to a few hundred microns a ribbon which has been previously drawn by some other process are high. Such processes do not at present appear feasible with the amount of shaping power that is likely to be available in a space processing facility.
8. It cannot be expected that electromagnetically shaped ribbon will be of uniform thickness. The thickness near the ribbon center could easily be twice that near the edges. This might not lead to major problems in applications, but could be a problem in keeping the ribbon from touching the shaping coils.
9. Shaping coils could be cooled satisfactorily by convective transfer to fluid flowing through a hollowed wire, and possibly by other means.
10. Eddy-current heating of the molten silicon will raise its temperature significantly and will move the liquid-solid interface rather far from the region of maximum shaping force, under typical shaping conditions, unless some form of substantial auxiliary cooling of the ribbon can be provided.
11. In the absence of electromagnetic forces, the principal mechanism determining the shape of liquid silicon in the space environment is capillarity, which dominates over viscous, accelerational, or flow forces. The morphology of the liquid silicon is thus principally dependent on the shape of any solids with which it comes into contact and the equilibrium contact angles between the silicon and the materials of these solids. Ribbon could in principle be produced simply by drawing between parallel wires.
12. The rate of ribbon production, the homogeneity of the solid material produced, and the thinness of the shaped ribbon can all be enhanced by a process of off-angle growth in which the ribbon is pulled at an angle to the direction of solidification.

On the basis of these findings, we make the following recommendations:
1. Although a number of possible difficulties in and drawbacks to space production of silicon single-crystal ribbon have been identified, nothing has been found which definitely nullifies the technical feasibility of such a process. Therefore we do not recommend that work in this area be halted. In view of the overall importance of being able to produce high-quality silicon ribbon at reasonable expense, I recommend that work along these lines continue to the extent justified by the overall goals of the space-processing program.

2. The concepts of greatest promise, both with regard to electromagnetic shaping and to other methods, are very "space-oriented" and there is no reason to believe they can be convincingly demonstrated or modeled on earth. Obviously, therefore, terrestrial experiments cannot be generally recommended, although some experiments to test a particular point might be desirable. For example, it appears that a realistic investigation and test of many aspects of the capillarity-driven shaping concept described in Sec. 3.3 could be carried out on earth using immiscible liquids of similar densities, as in the classic experiments of Plateau.[32]

3. A number of specific problems associated both with electromagnetic and non-electromagnetic shaping of ribbon have been pointed out in the conclusions above and elsewhere in the report. The primary need at the present time is for innovative conceptualization to develop practicable ways these problems might be dealt with. If and when such ideas are formulated, further modeling to obtain a more quantitative assessment of their validity would be called for. Only after development of a demonstrably sound procedure for ribbon shaping would further design of the overall space processing system appear appropriate.

5. REFERENCES

1. F. A. Padovani and F. W. Voltmer, Texas Instruments, Inc., Report NASA-CR-124439 "Growth of a Single Crystal Ribbon in Space", to NASA-Marshall Space Flight Center, 1973.
2. W. R. Marx et al, McDonnell-Douglas Astronautics Company, "Feasibility Study of Commercial Space Manufacturing," Report to NASA-Marshall Space Flight Center on Contract NASA-8-31353, May 1975.
3. M. Olette, Comptes Rendus 244, 1033 (1957).
4. R. A. Logan and W. L. Bond, J. Appl Phys, 30, 322 (1958).
5. Yu. M. Shashkov and V. P. Grishin, Soviet Phys.--Solid State 8, 447 (1966).
6. Y. S. Touloukian, R. W. Powell, C. Y. Ho, and P. G. Klemens, Thermal Conductivity (vol. 1, Thermophysical Properties of Matter Series) (IFI/ Plenum Press, 1970), p. 339.
7. V. M. Glazov, S. N. Chizhevskaya, and N. N. Glagoleva, Liquid Semiconductors (Plenum Press, 1969), p. 60.
8. P. H. Keck and W. VanHorn, Phys. Rev. 91, 512 (1953).
9. R. J. Jaccodine, J. Electrochem. Soc. 110, 524 (1963).
10. V. M. Glazov, Izvest. Akad. Nauk SSSR, Otdel. Tekhn. Met. i Tepl., #5, 110 (1962); J. R. Wilson, Met. Revs. 10, 381 (1965).
11. R. Rochat, McDonnell-Douglas Corporation (private communication).
12. M. Neuberger and S. J. Welles, Silicon, Electronic Properties Information Center Report DS-162 (1969), p. 134, quoting work of V. F. Brekovskikh.
13. Y. S. Touloukian, R. W. Powell, C. Y. Ho, and M. C. Nicolaou, Thermal Diffusivity (vol. 10 in Thermophysical Properties of Matter Serice) (IFI/ Plenum Press, 1973), p. 160.
14. G. K. Gaule and J. R. Pastore, in Metallurgy of Elemental and Compound Semiconductors, R. O. Grubel, ed. (Interscience Publishers, 1961), p. 201.
15. R. L. Stoll, The Analysis of Eddy Currents (Oxford Univ. Press, 1974), Chap. 1.
16. H. Poritsky and R. P. Jerrard, Trans. AIEE 73, (I), 97 (1954).
17. R. L. Stoll, Ref. 15, Chap. 4.

REFERENCES
(Cont.)

18. A. Erdelyi et al, Tables of Integral Transforms, Vol. I, (McGraw-Hill, 1954).
19. M. Abramowitz, Chap. 12, Handbook of Mathematical Functions, M. Abramowitz and I. A. Stegun, eds., (NBS Applied Mathematics Series #55, U.S. Department of Commerce, Washington, 1964).
20. F. W. J. Olver, Chap. 9, Handbook of Mathematical Functions, Ref. 9.
21. A. H. Stroud, Approximate Calculation of Multiple Integrals (Prentice-Hall, 1971), Sec. 2.3.
22. L. M. Milne-Thomson, Chap. 17, Handbook of Mathematical Functions, Ref. 9.
23. R. L. Stoll, Ref. 15, Chap. 2.
24. R. L. Stoll, Ref. 15, Chap. 8; R. L. Stoll, Proc. IEE 114, 775 (1967).
25. H. S. Carslaw and J. C. Jaeger, Conduction of Heat in Solids, 2nd ed., Chap. VII (Oxford Univ. Press, 1959).
26. M. Fishenden and O. A. Saunders, An Introduction to Heat Transfer, Chap. VI, (Oxford Univ. Press, 1950).
27. S. Whitaker, J. Amer. Inst. Chem. Eng. 18, 3611 (1972).
28. S. Strella, J. Appl. Phys. 41, 4242 (1970).
29. A. J. Markworth and M. L. Glasser, J. Appl. Phys. 46, 2327 (1975).
30. W. C. Reynolds, Report LG-1, Stanford University, Stanford, California (Sept. 1961).
31. E. W. Otto, "Static and Dynamic Behavior of the Liquid-Vapor Interface During Weightlessness," in Aerospace Chemical Engineering, Chem. Eng. Progr. Symposium Series, No. 61, Vol. 62 (1966), p. 158.
32. J. C. C. Nitsche, Amer. Math. Monthly 81, 945 (1974).
33. Ta Li, J. Chem. Phys. 36, 2369 (1962).
34. W. A. Darbro, "Research on Solidification of Liquids Suspended on Boundaries in Zero-G," Unpublished NASA-MSFC manuscript (May, 1975).
35. W. Darbro, "Liquid Film Demonstration Experiment--Skylab SL-4," NASA-MSFC Technical Memorandum NASA TM X-64911, (January, 1975).
36. A. J. Markworth and W. Oldfield, "Study of Ceramic Products and Processing Techniques in Space," Final Report to California Institute of Technology, Jet Propulsion Laboratory, Pasadena, California (December 1, 1974).